ENG 261-(EQC 1991/10)

Behaviour Of Cold-Formed Steel RHS Members under Cyclic Loading

Warren R Walpole, Department of Civil Engineering, University of Canterbury

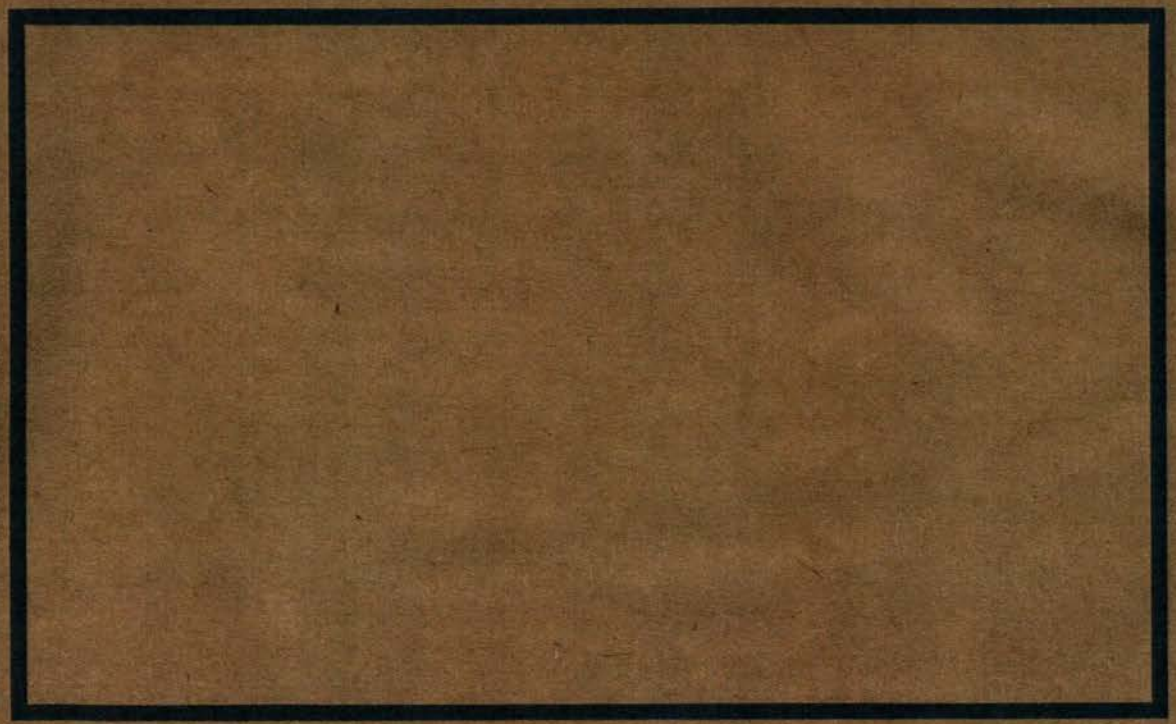

ISSN 0110–3326

RESEARCH REPORT

BEHAVIOUR OF COLD-FORMED STEEL RHS MEMBERS UNDER CYCLIC LOADING

Warren R. Walpole

November 1996 96-4

Department of Civil Engineering

University of Canterbury
Christchurch New Zealand

ISSN 0110-3326

Research Report

BEHAVIOUR OF COLD-FORMED STEEL RHS MEMBERS UNDER CYCLIC LOADING.

Warren R. Walpole

November 1996 96-4

Department of Civil Engineering
University of Canterbury
New Zealand

ABSTRACT

Three steel members and a stub column made from cold-formed rectangular hollow sections (RHS) were tested under cyclic axial tension and compression loading. The section tested was a 150 x 100 x 6 RHS with a specified yield stress of 350 MPa. Three different overall slenderness ratios were tested, 40, 60 and 80. Pin ended and fixed ended connections were tested. It was found that local buckling occurred relatively quickly and that the magnitude of the local buckles increased under repeated loading. Eventually this led to fractures developing at the sharp local buckles giving reduced ductilities. The ratio of the width to the thickness for the element of a cold-formed section allowed by NZS 3404 Steel Structures Standard may need to be reduced, where high ductility is required for design against earthquakes.

ACKNOWLEDGMENTS

This research has been supported by a grant from the Earthquake Commission.

Laboratory equipment and space were provided by the Civil Engineering Department. The assistance of departmental technicians in carrying out this research is gratefully acknowledged.

Dr Alexander Remennikov assisted in the calculation of the theoretical behaviour of the members using the "Brace model" computer routine [7].

LIST OF CONTENTS

LIST OF FIGURES

Chapter 4 :Theoretical modelling

Chapter 5: Comparison of experimental tests and theory

Chapter 6: Discussion

CHAPTER 1

INTRODUCTION

Steel members are frequently required to be designed to carry tension and compression loading, especially the braces in concentrically-braced frames. Under the action of an earthquake, cyclic loading may occur and depending on the magnitude of the lateral loads, compared to the design forces, yielding in tension and buckling in compression could occur. This report describes the testing of members made from rectangular hollow sections (RHS), where the loading reversed between tension and compression. RHS have relatively high radii of gyration r and hence may be an economical section to use as a brace member. This shape is produced by rolling a flat length of steel, so that the longitudinal edges may be welded together, and a rectangular cross-section produced. In Australia and New Zealand the RHS is cold-formed, to produce the required rectangular or square shape. It is possible to import RHS from the UK that has been hot-rolled to shape. The cold-forming process will induce a different pattern of residual stress, within the section compared to a hot-rolling process. Lower limits are set by NZS3404:1992 [1] for the slenderness of elements of sections, which have been cold-formed, compared to those sections, which have been hot-rolled. Another type of section, used as a brace member, is the Universal Column (UC) section. Earlier Leowardi [2] tested three UC members and a stub column, under cyclic loading. It was found that the behaviour could be predicted with reasonable accuracy using a physical theory, from the variation of the tangent modulus with cyclic loading, obtained in a stub column test. The physical theory may be developed from the simple model shown in Figure 1.1, where the plastic hinge is considered to form at a point, while the rest of the member remains elastic. This report describes the recent testing of three RHS members and a stub column.

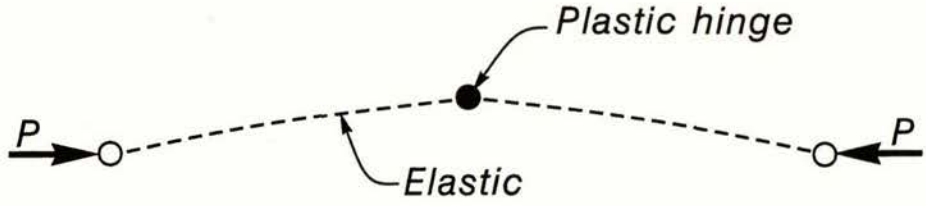

Figure 1.1 Physical model of brace

CHAPTER 2

EXPERIMENTAL PROGRAMME

Yield tests

The members and stub column were all made from the one length of cold-formed 150 x 100 x 6 RHS. Three samples were taken from the flat part of the section, so that the experimental yield test could be obtained. The variation of applied stress versus strain is shown in figures 2.1, 2.2 and 2.3 for coupons T1, T2 and T3 respectively. The 0.2% strain offset line was found by drawing a line from the point corresponding to a strain of 0.002 and zero stress. The line was drawn at a slope of the elastic Young's modulus 200 GPa. The yield stress was determined by finding the intersection point between the 0.2% strain offset line and a regression curve drawn as the line of best fit to the experimental points. This is the conventional procedure for determining a proof stress, when the stress-strain curve shows gradual yielding. In addition, the stress on the regression curve at a strain of 0.05 was found and later used as the yield stress in the theoretical prediction of the behaviour of the members, because it was found to give curves which more closely matched the experimental curves. This stress is typical of the values of stress on the long plateau found for the stress-strain curve for the RHS. The material did not exhibit any strain hardening, nor any distinctive yield point. Yielding occurred gradually, and then after a long plateau of fairly constant stress, fracture eventually took place. The values of yield stress for the three samples and the average values are given in Table 2.1.

Table 2.1

Sample	Yield stress MPa	
	Strain for yield stress	
	0.002	0.05
T1	453	484
T2	461	498
T3	432	489
Average	449	490

Test Specimens

Three steel brace members and a stub column, made from a cold-formed rectangular hollow steel section, were tested under cyclic axial tension and compression loading, in the DARTEC universal testing machine in the Civil Engineering Laboratory, at the University of Canterbury. The section tested was a 150 x 100 x 6 RHS with a specified minimum yield stress f_y of 350 MPa. The experimental yield stresses were significantly higher than the specified minimum value, as detailed above. This section has a width to thickness ratio (d-2t)/t of 23.0 for the longer side. NZS3404:1992 defines the element slenderness λ_e as follows:

$$\lambda_e = \frac{b}{t}\sqrt{\frac{f_y}{250}} = \frac{d-2t}{t}\sqrt{\frac{f_y}{250}}$$

where

- b = clear width of a supported element between the faces of supporting plate elements
- d = overall depth
- t = thickness
- f_y = yield stress

The NZ code specifically excludes allowance for the curved corners of the section, when the width b is calculated. This is unusual, but presumably this is done to simplify the calculation of the width of plate panels. It is inconsistent with the definitions of well-established cold-formed codes, such as the AISI code [3]. λ_e for the specimens is given in Table 2.2 below, for the specified and test values of f_y. The limit $\lambda_{e1,2}$ given by Table 12.5 of NZS3404:1992 is 30 for full or limited ductility members and the limit λ_{e3A} for members that remain nominally elastic is 40. The section therefore complies with the current limits, for both $\lambda_{e1,2}$ and λ_{e3A} in NZS 3404:1992, using the specified minimum yield stress when calculating λ_e, but would not comply with the limit $\lambda_{e1,2}$ for full or limited ductility, if the real experimental yield stress values were used.

Table 2.2

Yield stress MPa		Element slenderness λ_e
Specified minimum	350	27.2
Average test value at 0.002 strain	449	30.8
Average test value at 0.05 strain	490	32.2

NZS 3404:1992 defines the modified slenderness ratio λ_n as follows:

$$\lambda_n = \frac{L_e}{r}\sqrt{k_f}\sqrt{\frac{f_y}{250}}$$

where L_e = Effective length

k_f = Form factor

r = Radius of gyration

The United States AISC Seismic Provisions for Structural Steel Buildings - Load and Resistance Factor Design [4] limits the ratio of the flat width b to the wall thickness t for members of concentrically-braced steel frames to the following:

$$\frac{b}{t} = \frac{110}{\sqrt{f_{y(ksi)}}} = \frac{289}{\sqrt{f_{y(MPa)}}}$$

where b = width of the flat portion of the panel

This limit is 15.4 for Grade 350 steel. The 150 x 100 x 6 RHS has a flat width to thickness ratio of 22. Hence the sections tested would not comply with the requirements of the 1990 AISC Seismic Provisions. This section was the thickest of three, within a group with the same overall depth and width. There are many RHS sections that do not comply with the limit on $\lambda_{1,2}$ in NZS3404. (In addition, very few

of the RHS or SHS listed in the Australian AISC Tables would comply with the American limit.)

Figure 2.4 shows the stub column and three members that were tested. Table 2.3 summarises the lengths, end conditions and modified slendernesses λ_n for the test specimens. The modified slendernesses are calculated for both the specified minimum yield stress and the experimental 0.2% proof yield stress. The pin-ended specimens were bolted to cleats, that were pinned to clevises bolted to the test machine; whereas the fixed-ended specimen and the stub column were bolted directly to the machine cross-head and the actuator.

Table 2.3

Specimen #	Specimen Length (mm)	End Conditions	Effective Length (mm)	L_e/r_y	Modified slenderness λ_n for f_y from	
					Test	Specification
1	2064	Pin-Pin	2704	67.6	94.7	80
2	1388	Pin-Pin	2028	50.7	71.0	60
3	2704	Fixed-Fixed	1352	33.8	47.3	40

Loading regime

The specimens were subjected to the axial deformations listed in Table 2.4 and shown graphically in Figure 2.5 to 2.12 for the stub column and specimens #1, #2, and #3 respectively. The imposed axial displacements are listed in millimetres in Table 2.4 and in terms of axial ductilities in Table 2.5 using the 0.2% proof stress to determine the strain at ductility one.

Table 2.4

Imposed axial displacements (mm)

Cycle	RHS#stub	RHS#1	RHS#2	RHS#3
	0.5	1.8	1.2	2.4
1	-0.5	-2.0	-1.3	-2.6
	0.9	3.7	2.3	4.9
2	-0.9	-3.8	-2.5	-5.1
	1.8	7.5	4.8	9.9
3	-1.8	-8.0	-5.2	-9.9
	2.7	11.3	7.0	14.8
4	-2.7	-11.8	-7.4	-15.0
	3.6	15.0	9.40	19.8
5	-3.6	-15.7	-9.64	-20.1
	4.5	19.0	11.9	25.3
6	-4.7	-19.4	-12.6	-24.4
	8.9	37.9	23.0	19.3
7	-8.9	-39.6	-24.2	
	13.3	31.0	24.2	
8	-13.4			
	17.7			
9	-17.7			

Table 2.5

Ductilities from experimental yield stress

Cycle	RHS#stub	RHS#1	RHS#2	RHS#3
	0.45	0.39	0.39	0.40
1	-0.45	-0.43	-0.42	-0.43
	0.80	0.80	0.74	0.81
2	-0.80	-0.82	-0.80	-0.84
	1.61	1.62	1.54	1.63
3	-1.61	-1.73	-1.67	-1.63
	2.41	2.44	2.25	2.44
4	-2.41	-2.55	-2.37	-2.47
	3.21	3.24	3.02	3.27
5	-3.21	-3.39	-3.10	-3.31
	4.01	4.10	3.82	4.17
6	-4.19	-4.19	-4.05	-4.02
	7.94	8.19	7.39	3.18
7	-7.94	-8.56	-7.77	
	11.86	6.70	7.77	
8	-11.95			
	15.79			
9	-15.79			

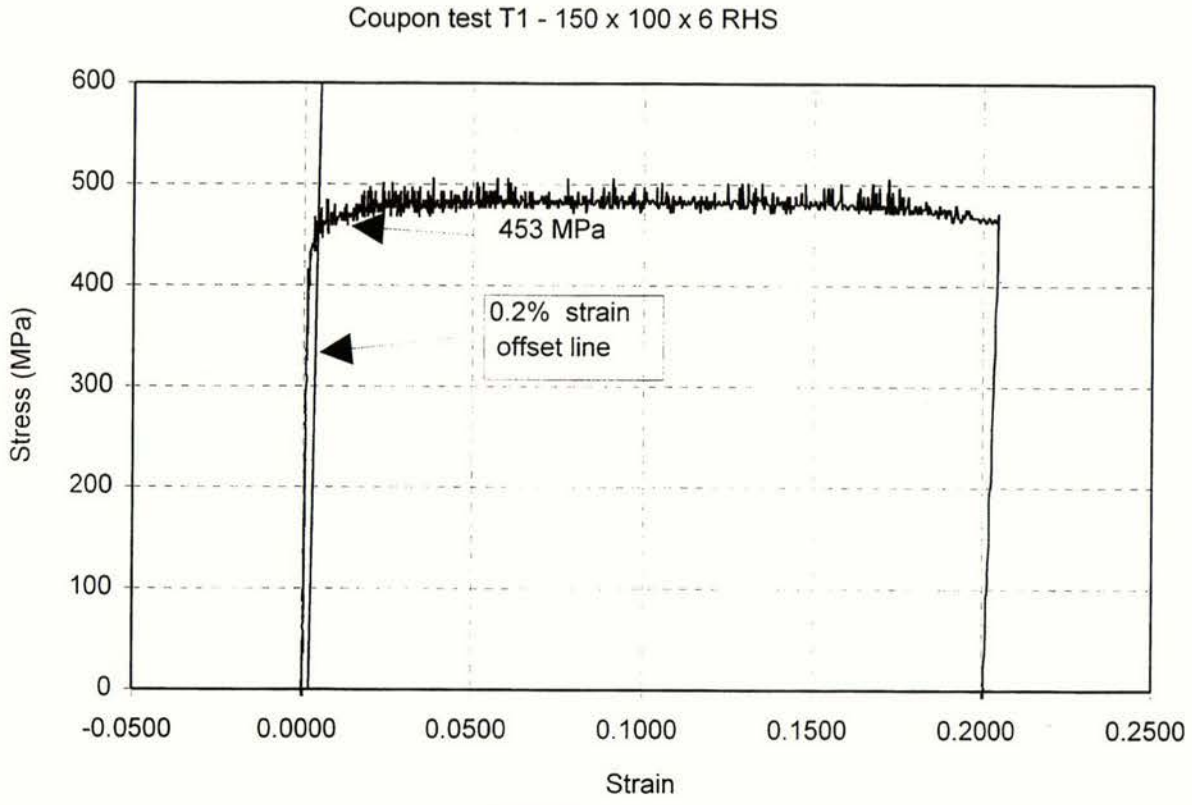

Figure 2.1 Coupon test #1 Stress versus strain

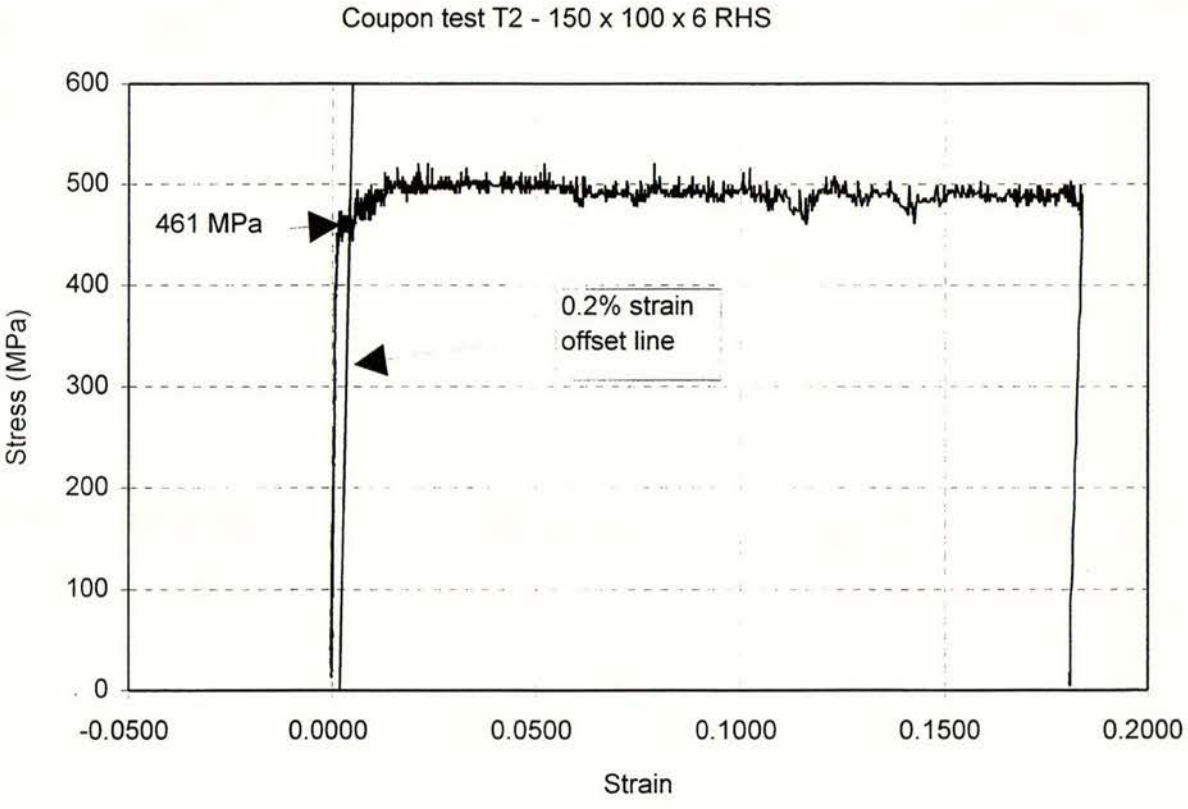

Figure 2.2 Coupon test #2 Stress versus strain

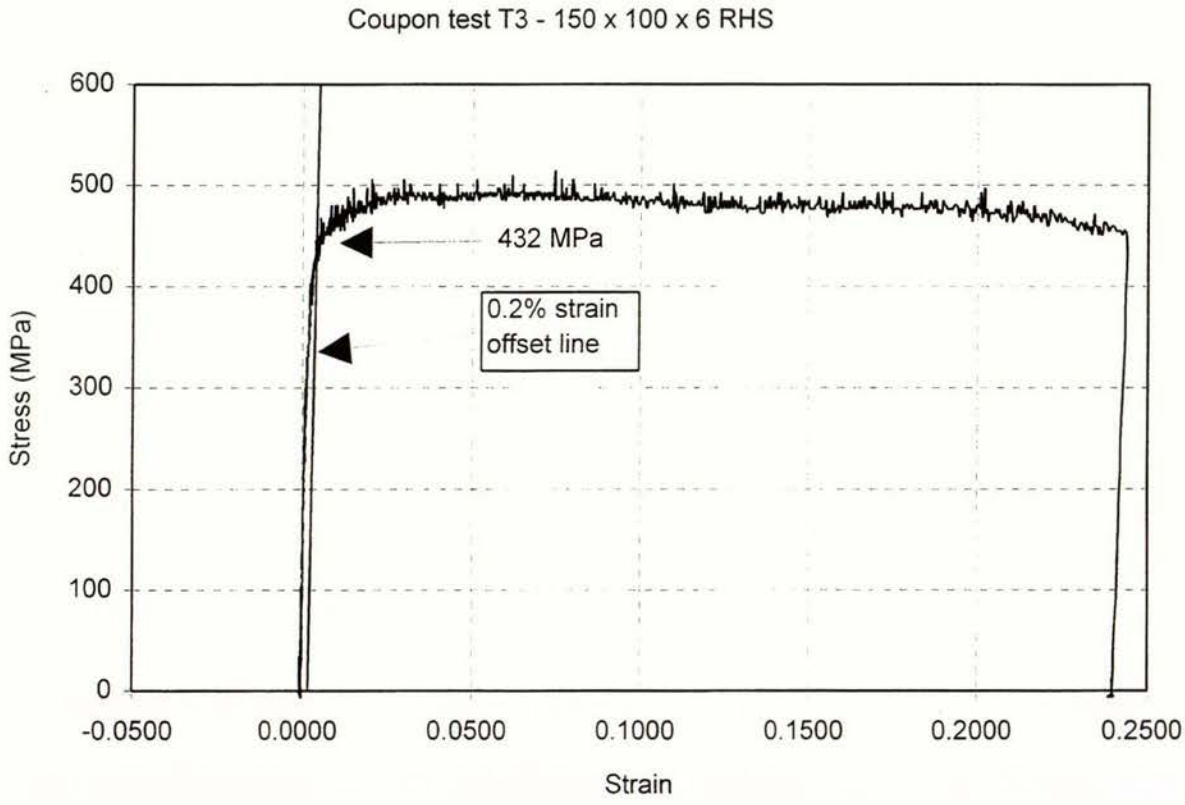

Figure 2.3 Coupon test #3 Stress versus strain

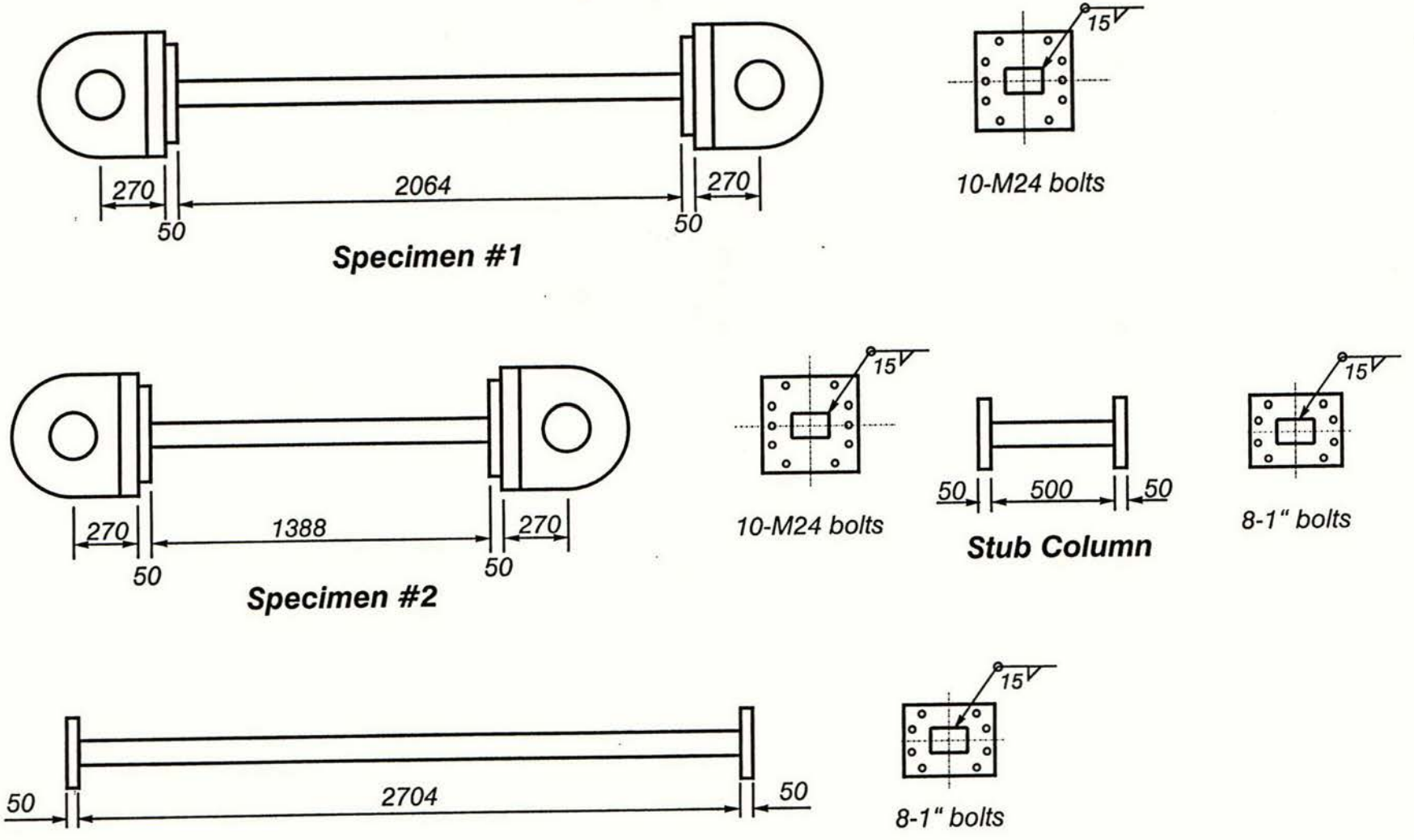

Figure 2.4 Test specimens

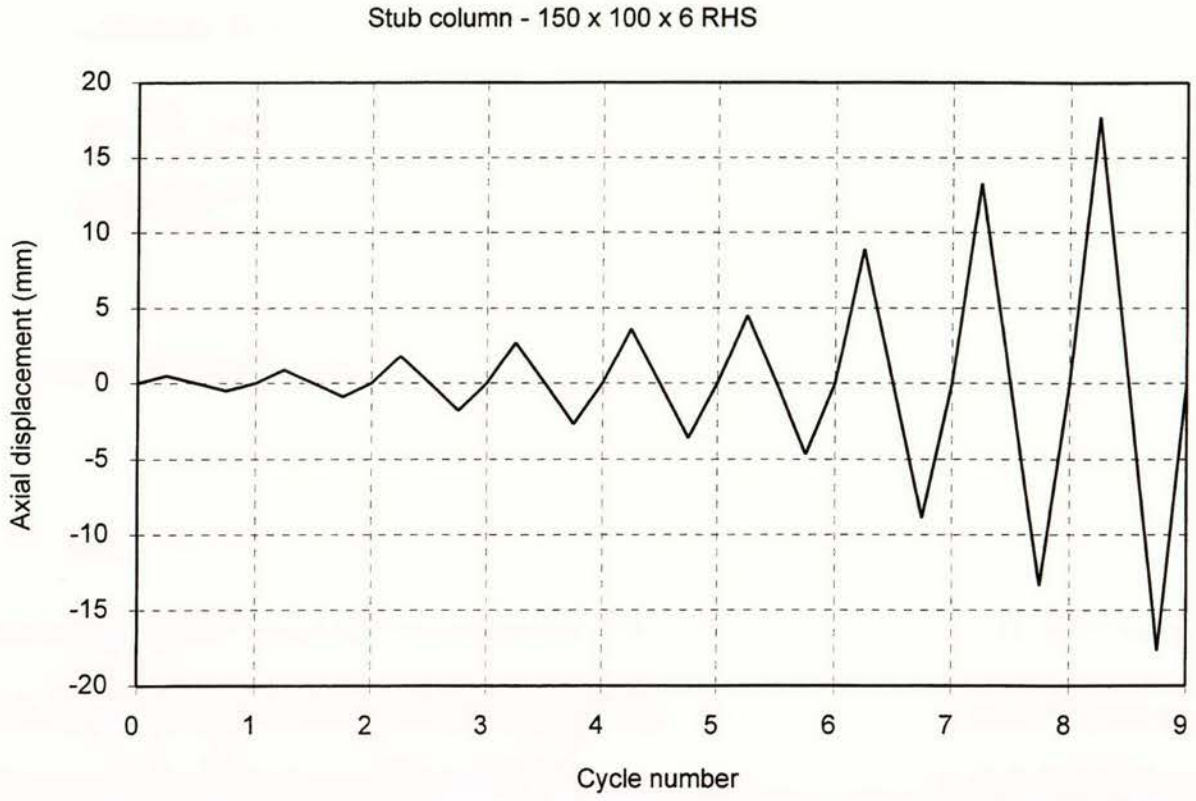

Figure 2.5 Stub column: axial displacement versus cycle number

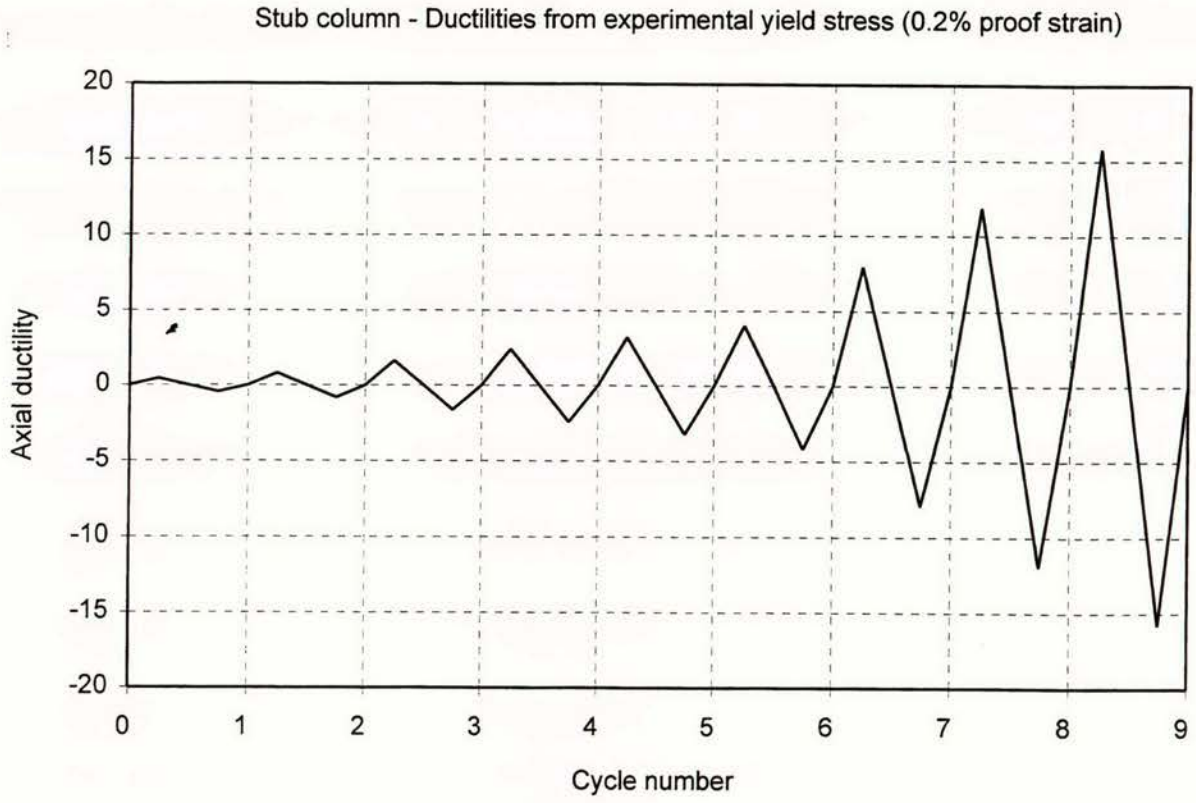

Figure 2.6 Stub column: axial ductility versus cycle number

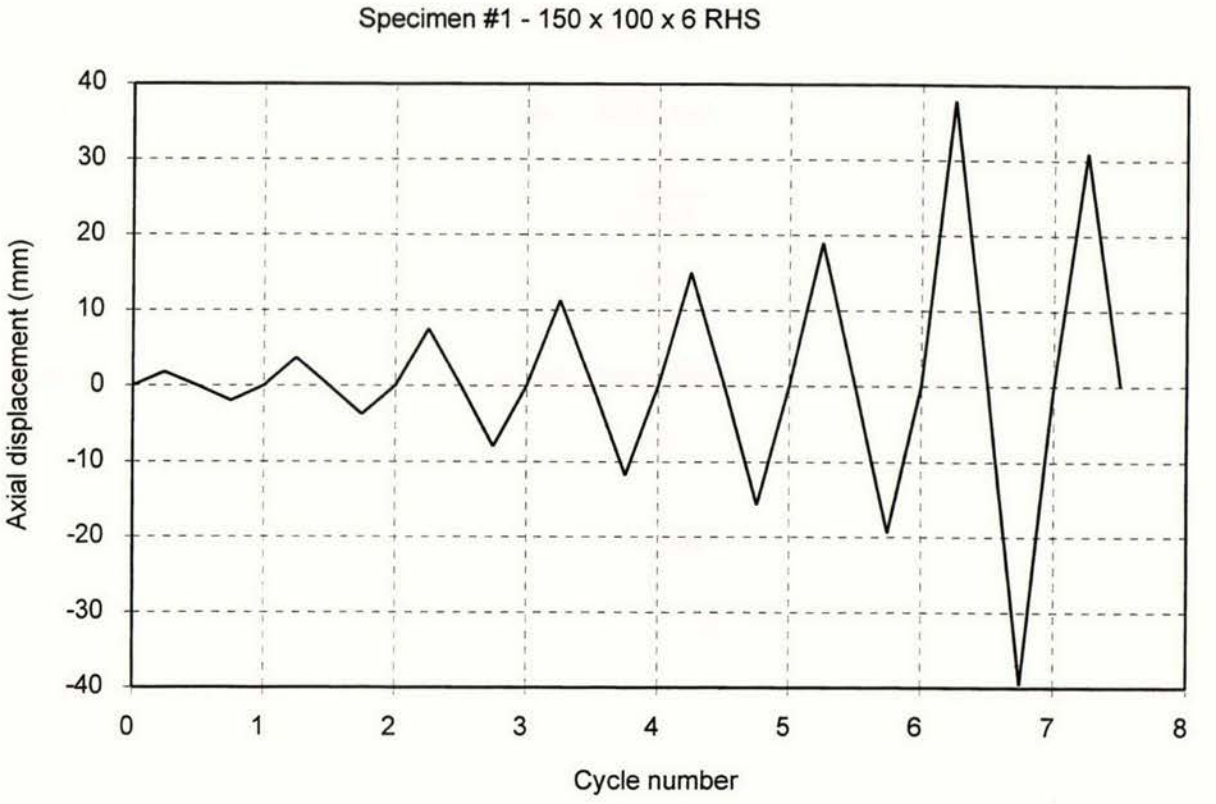

Figure 2.7 Specimen #1: axial displacement versus cycle number

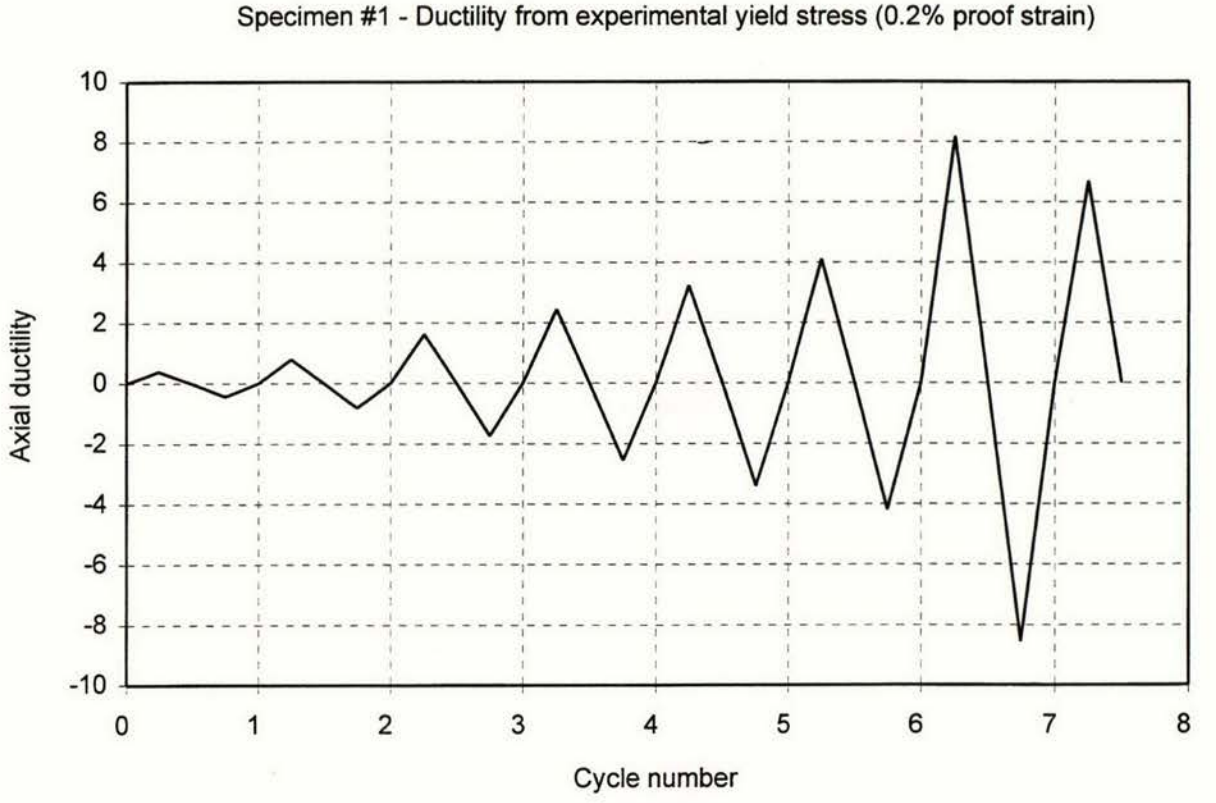

Figure 2.8 Specimen #1: axial ductility versus cycle number

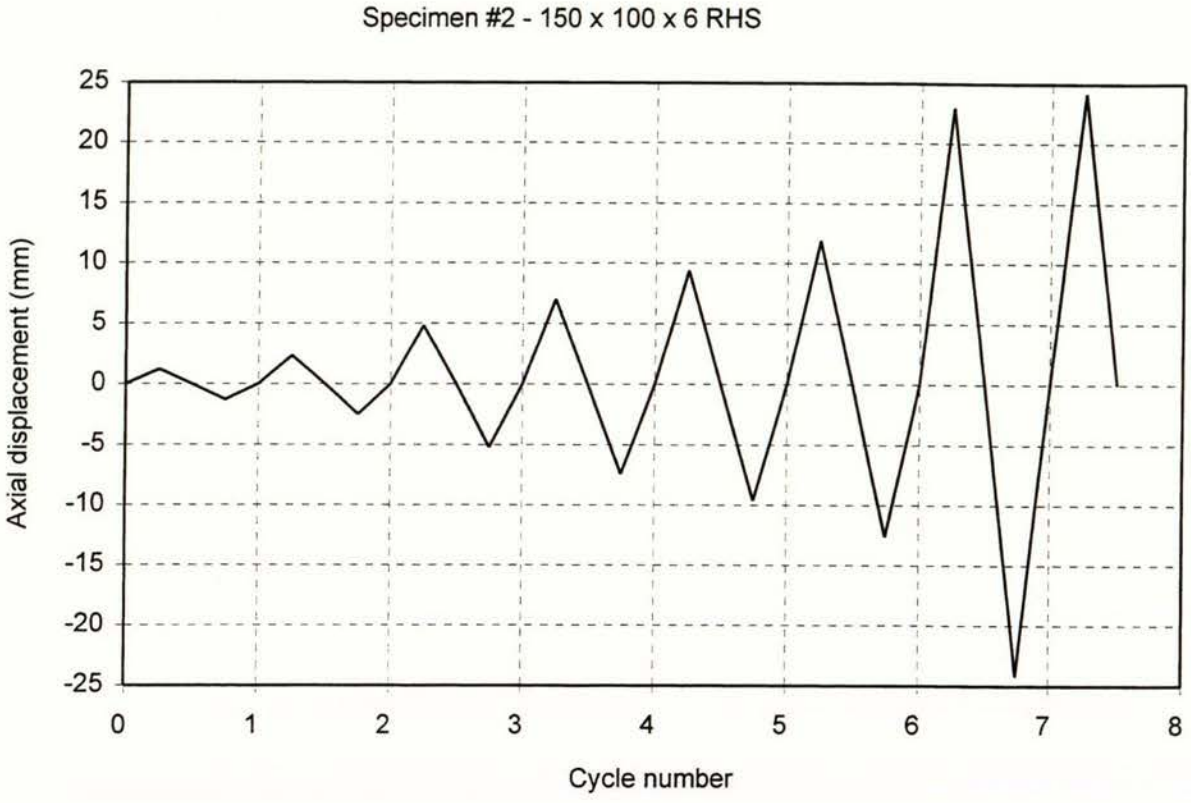

Figure 2.9 Specimen #2: axial displacement versus cycle number

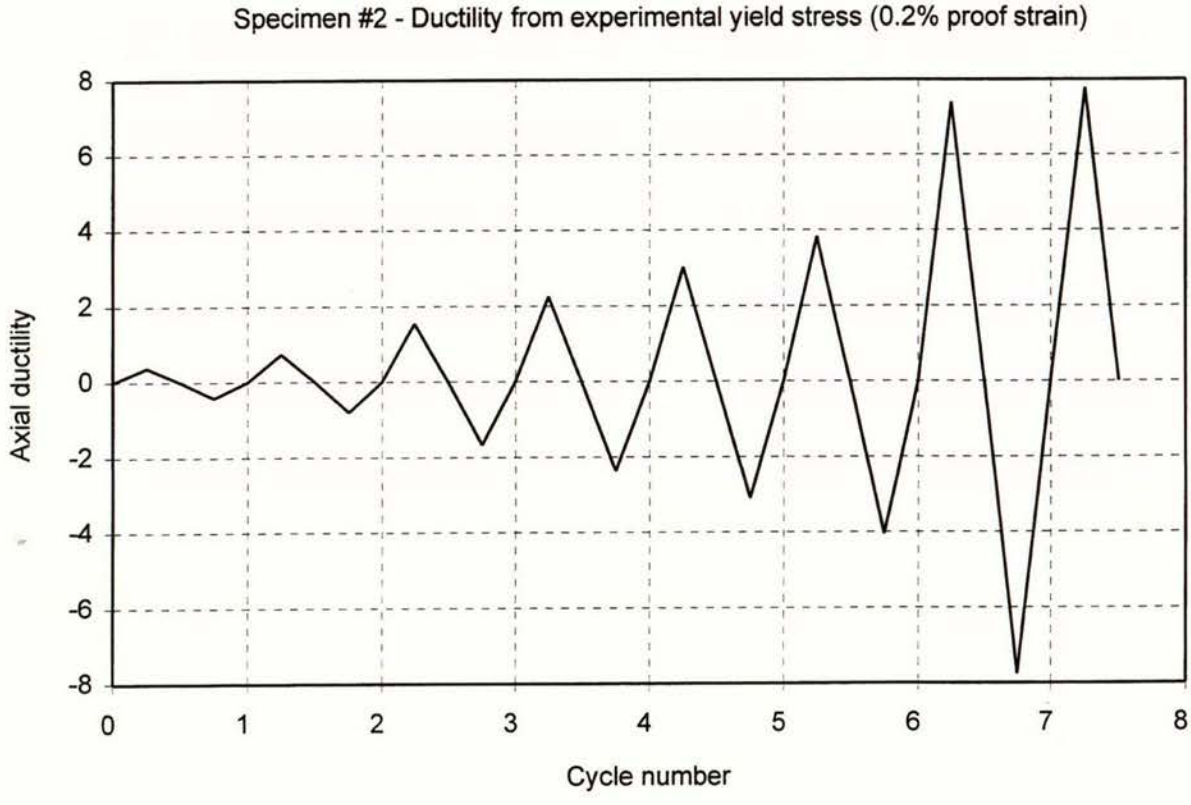

Figure 2.10 Specimen #2: axial ductility versus cycle number

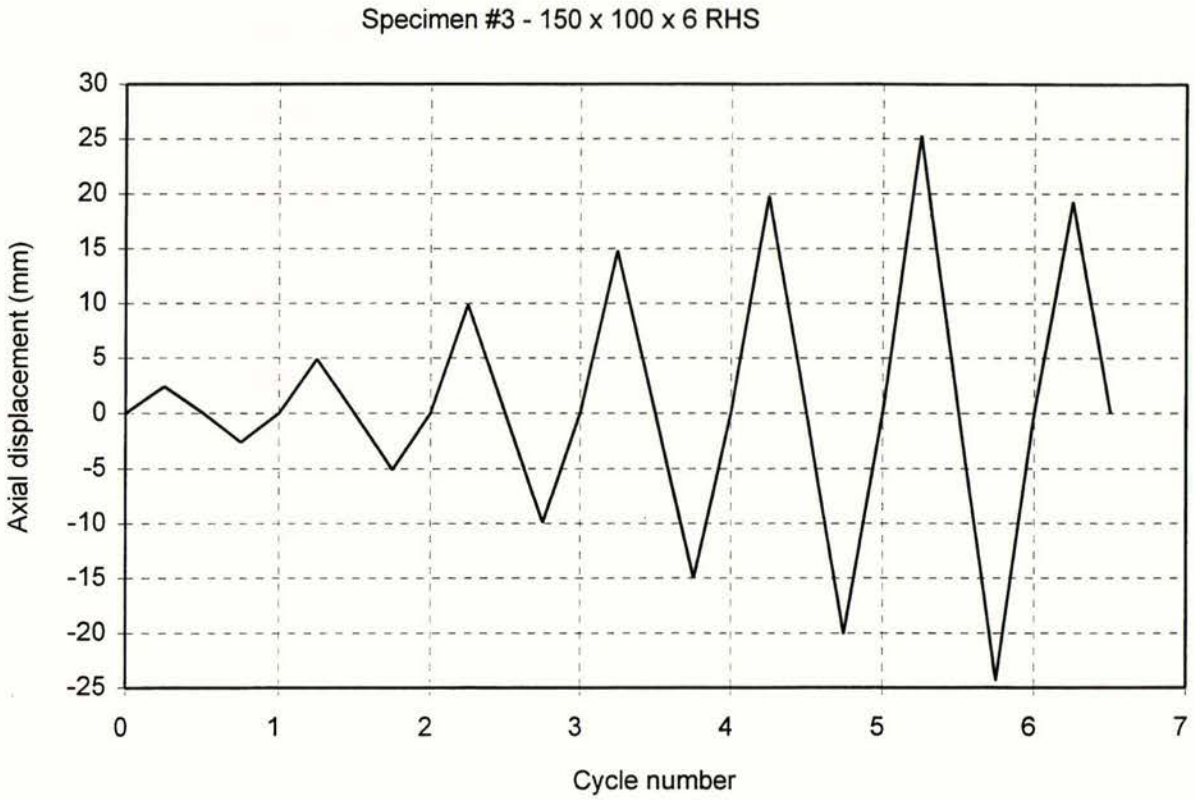

Figure 2.11 Specimen #3: axial displacement versus cycle number

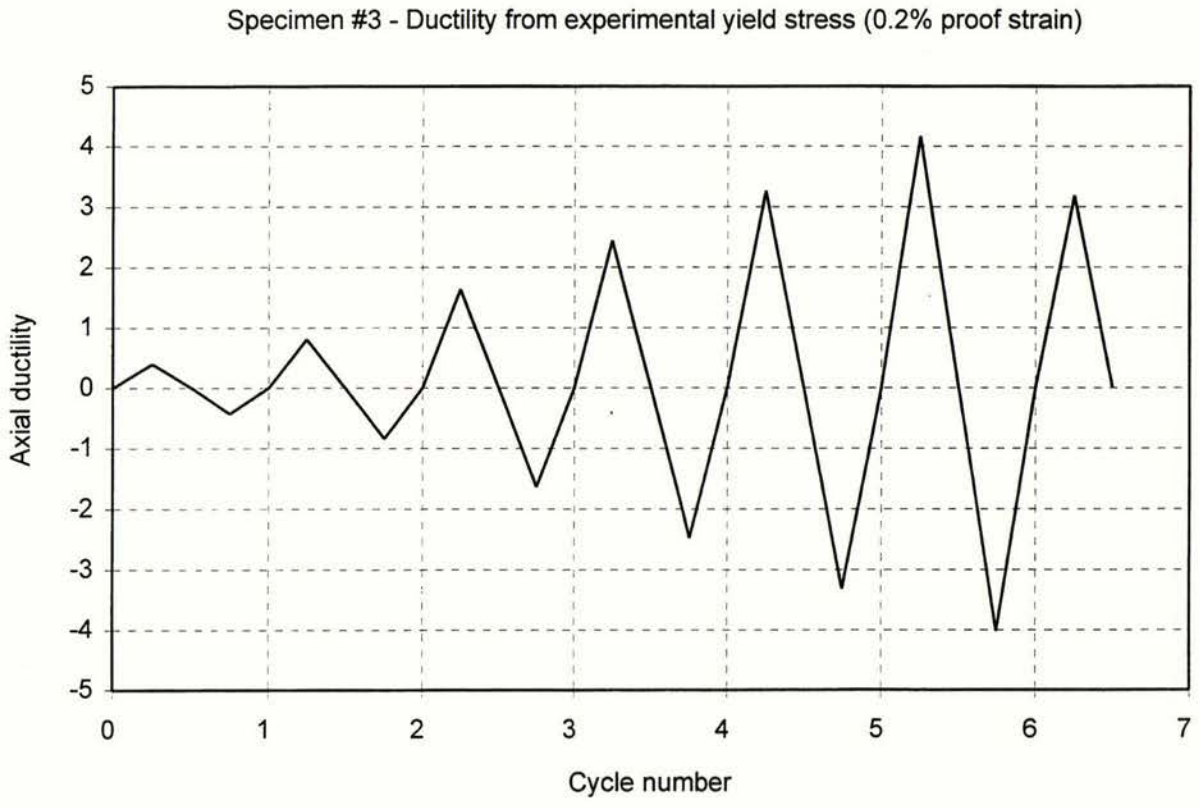

Figure 2.12 Specimen #3: axial ductility versus cycle number

CHAPTER 3

EXPERIMENTAL RESULTS

The test specimens were subjected to the axial deformations and axial ductilities detailed in the previous chapter, under displacement control. The axial ductility is calculated by dividing the axial extension by the extension of the member at yield, calculated using the test yield stress 449 MPa, at a strain of 0.002 and the elastic value of Young's modulus, 200 GPa. For all specimens, testing was stopped when a major crack appeared, that would precede total fracture of the section. The variation of the axial force P with the axial displacement δ during the tests for the stub column and specimens #1, #2 and #3 are shown in figures 3.1, 3.2, 3.3 and 3.4 respectively. Figure 3.5 and 3.6 show the variation of the test axial force with the moment at the centre of the member for specimens #1 and #3 respectively. Figure 3.7 and 3.8 show how the test axial force varied with the lateral displacement for specimens #1 and #3 respectively.

The stub column test was conducted to determine the variation of the tangent elastic modulus with cyclic loading, to enable the prediction of the theoretical behaviour of the test members. Generally the performance was very good with full hysteresis loops being obtained. However, local buckling reduced the peak compressive strength, during and after the 5th cycle when a displacement of –4.38 mm which corresponds to a ductility of –4.19, was reached, as shown in figure 3.1. This is a strain of 0.88%. The peak compressive forces were successively smaller with each cycle. There was some pinching of the deformation curve in tension during the 8th cycle, while the local buckle was being straightened. No cracks were formed in the local buckles, although ductilities of ±15.8 was reached. The modified slenderness of the stub column was only 8.7, to eliminate any overall buckling as a column. Figure 3.9 shows the stub column mounted in the DARTEC testing machine, when subjected to an axial shortening of 13.4 mm in the seventh cycle.

Specimen #1 performed well, reaching a ductility of -8.6 (-39.6 mm contraction, 1.92% strain) during the 7th cycle. The curves of axial force versus axial displacement showed excellent stiffness under tension, giving a large amount of energy adsorption. The maximum values were fairly constant in the last four cycles, but showed the typical loss of strength after overall buckling under compression. During the 4th cycle, the peak compression load was about -591 kN compared to the previous peak of -835 kN. This is the behaviour expected of brace members. During the 5th cycle the peak compressive load rose again to -820 kN. This is not typical of brace member behaviour. The peak compressive values in the 6th and 7th cycles increased to -919 kN and -945 kN. The member failed in the 7th cycle when the crack spread through the section. The tensile curve is pinched because of the need to straighten the local buckle and the overall buckle from a lateral displacement of 228 mm. Member #1 formed a local buckle in the plastic hinge region at mid-height during cycle 5 under an axial contraction of 15.7 mm, which corresponds to a ductility factor of -3.4. When the load was reversed and the member extended to an elongation of 19.0 mm (ductility 4.1), the member was straight, although the local buckle was just perceptible. After a cycle including ductility +8.19 and -8.56, cracks occurred in the corners of the section, when an elongation of 12 mm had been reached. This was followed soon after by fracture through the tensile side of the section, at an extension of 29.5 mm. Figure 3.10 shows specimen #1 when subjected to a contraction of 19.4 mm. Overall buckling and local buckling is evident. Figure 3.11 shows a closer view of the local buckle. The sharp curvatures at the edges of the buckle later caused fracture to occur. Figure 3.12 shows the member at the maximum axial contraction of -39.6 mm, with an axial ductility of -8.56, in the seventh cycle. Figure 3.13 shows a closer view of the local buckle shown in figure 3.12. When the loading was reversed the tensile force had to straighten the overall buckle and the local buckle. The sharp curvatures at the edges of the local buckle, near the RHS walls, caused small cracks. Under the tensile load in the final cycle, the crack grew longer and then spread right across the longer tensile side and around the corners of the RHS. Figure 3.14 shows the member at the end of the test. Figures 3.15 and 3.16 show close up views of the local buckle and fracture area.

Specimen #2 had full axial force versus axial displacement curves in tension. In compression, there was a significant loss of strength after the initial overall buckling had occurred. The strength dropped from -1051 kN at cycle three to -770 kN at cycle 4. During the 5th cycle, the strength dropped to -686 kN and then at cycle 6 the loss of strength was smaller again to -656 kN. This is the behaviour expected of a brace member. In the penultimate cycle 7 to ductility 7.8 there was a slight gain in magnitude of compressive strength to -670 kN, but the specimen failed in tension in the next cycle. Member #2 also formed a local buckle, that grew in magnitude as the number of cycles increased. Although the tensile loads tended to straighten the local buckle, it was not entirely removed and the next compressive cycle caused it to grow to a larger size. Figure 3.17 shows the member after overall buckling has taken place and a local buckle has formed at mid-height, during cycle seven. Figure 3.18 shows a closer view of the local buckle. When one cycle which included ductilities of 7.4 and -7.8 had been applied, fracture occurred through one side of the section at an axial elongation of 24 mm, which corresponded to a ductility of 7.8. Figure 3.19 shows the specimen at the end of the test, with a fracture through the tensile part of the section. Figure 3.20 shows a closer view of the fracture area.

Specimen #3 had the lowest modified slenderness of 47.3. The hysteresis loops are well rounded with no pinching of the loops up to cycle four. In cycle five there was a little pinching in compression, after reaching the peak compression buckling load. The was a bit more pinching of the curve in compression in cycle six. In cycle seven, there was significant degradation of strength, before the test was stopped. It formed a local buckle at a ductility factor of -3. The test was stopped when a major crack formed during tensile loading, after one cycle at ductility four. The ductilities were calculated using the experimental yield stress, based on a 0.2% proof strain. The experimental yield stress was significantly higher, than the specified minimum yield stress. The local buckling was more significant with this less slender specimen. Figure 3.21 shows the member after overall buckling and local buckling have occurred in cycle five, under an axial contraction of -20 mm. Figure 3.22 shows a closer view of the local buckle, formed in the plastic hinge region at mid-height. This specimen was fixed at the top and bottom to the test machine. It also formed plastic hinges at the top and bottom of the specimen and local buckling occurred in

these areas too. Figure 3.23 shows the local buckling, which occurred at the bottom of the specimen. The peak compressive load reached by specimens #2 and #3 was higher than that reached by specimen #1. Specimen #3 suffered a less rapid loss of strength than the other specimens, once overall flexural buckling had occurred, as shown in figure 3.4. The behaviour was very good during the first six cycles, but failure occurred at a relatively low ductility. The axial ductility was significantly reduced for this specimen, which had less flexural slenderness, because of the relatively earlier occurrence of the local buckling and the subsequent tensile fracture caused by the high strains associated with the sharp curvatures near the local buckle. Figure 3.24 shows the specimen near the end of the test in cycle seven at an elongation of 19.3 mm. The crack across the tensile side of the member is visible at mid-height.

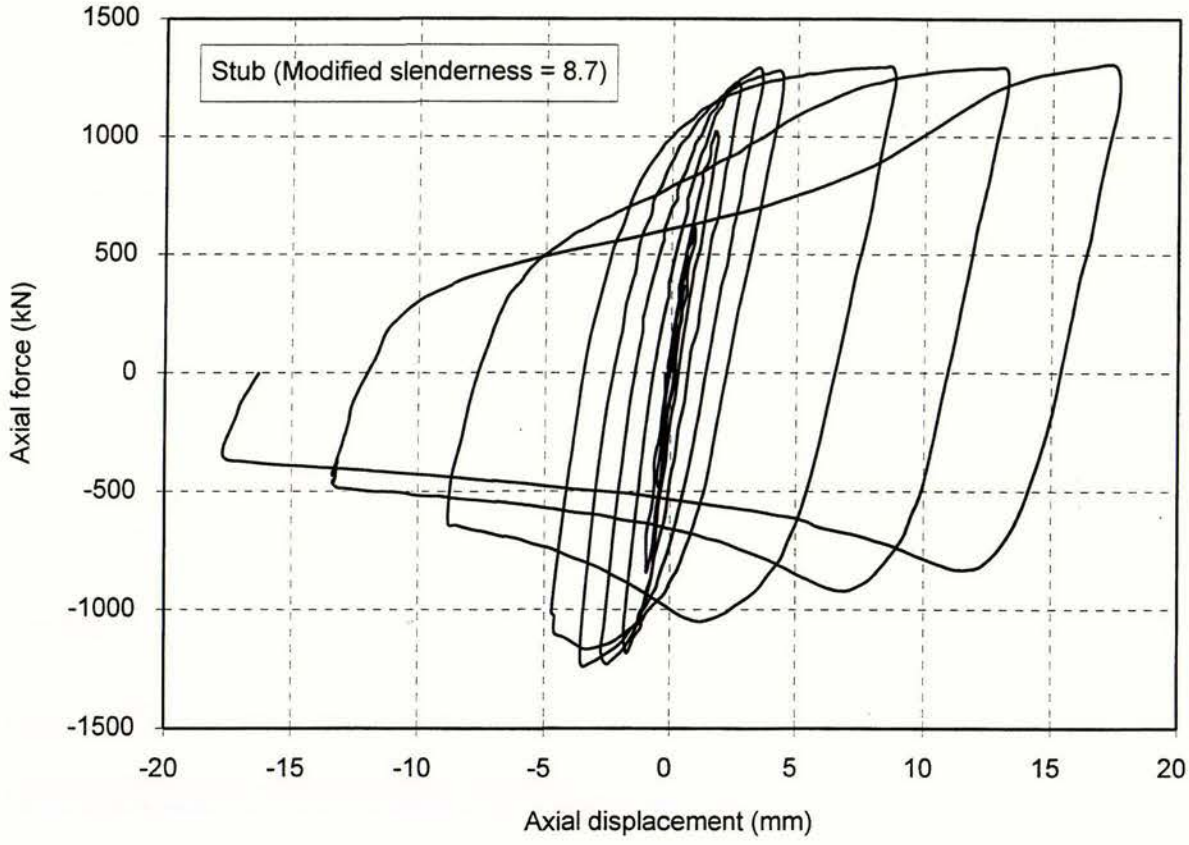

Figure 3.1 Stub column: Test axial force versus axial displacement

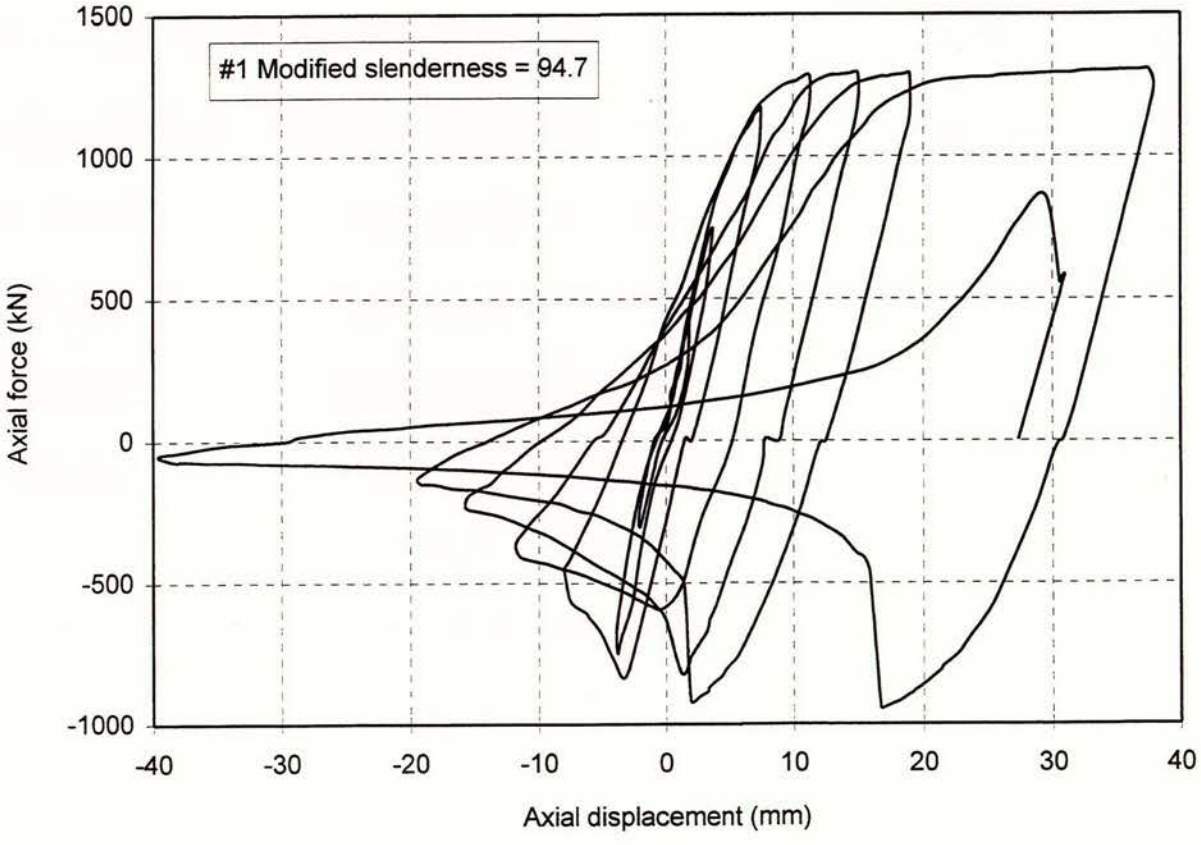

Figure 3.2 Specimen #1: Test axial force versus axial displacement

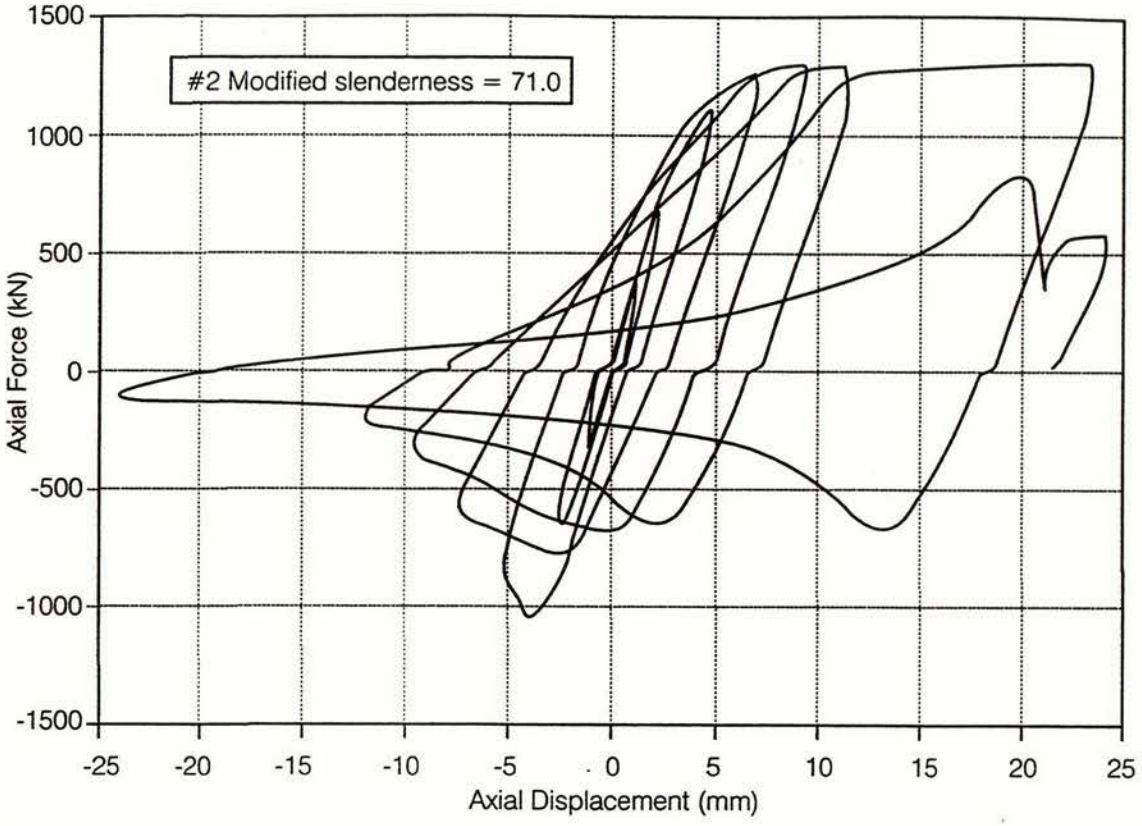

Figure 3.3 Specimen #2: Test axial force versus axial displacement

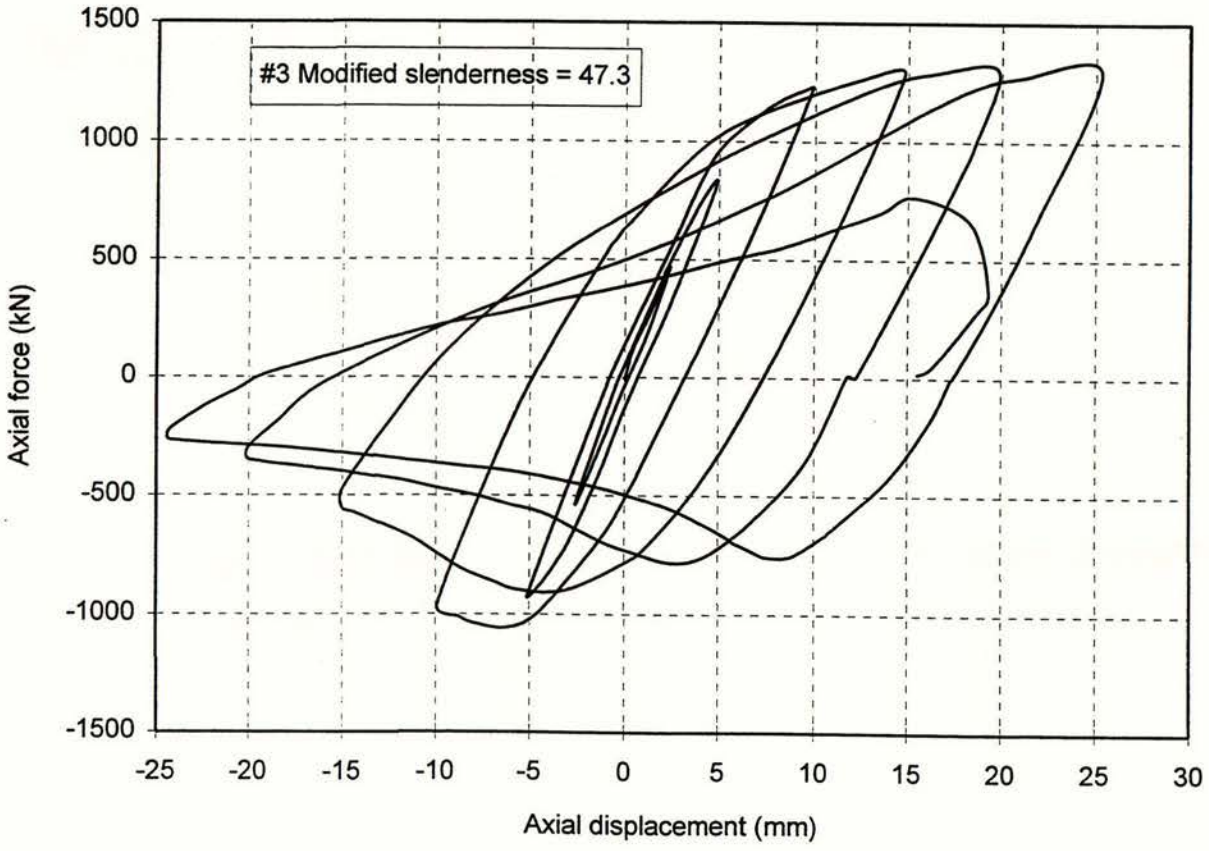

Figure 3.4 Specimen #3: Test axial force versus axial displacement

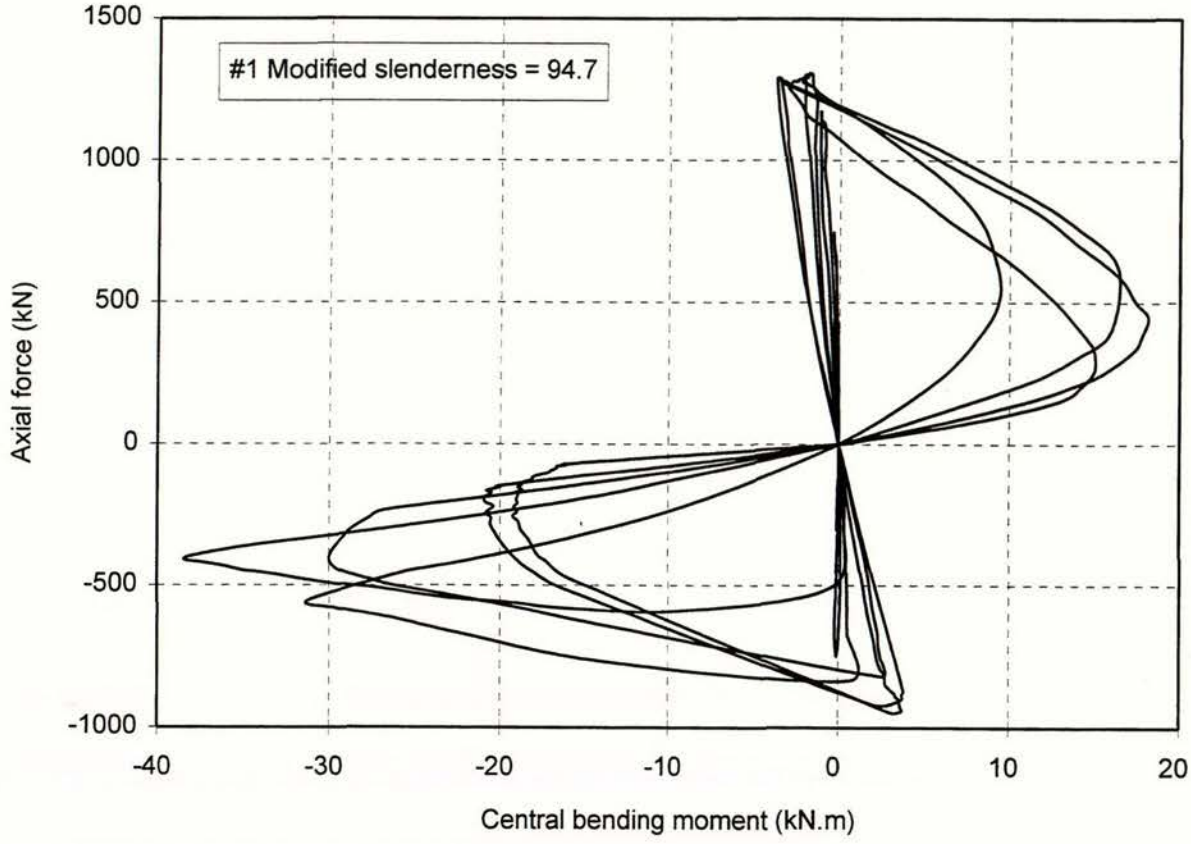

Figure 3.5 Specimen #1: Test axial force versus central bending moment

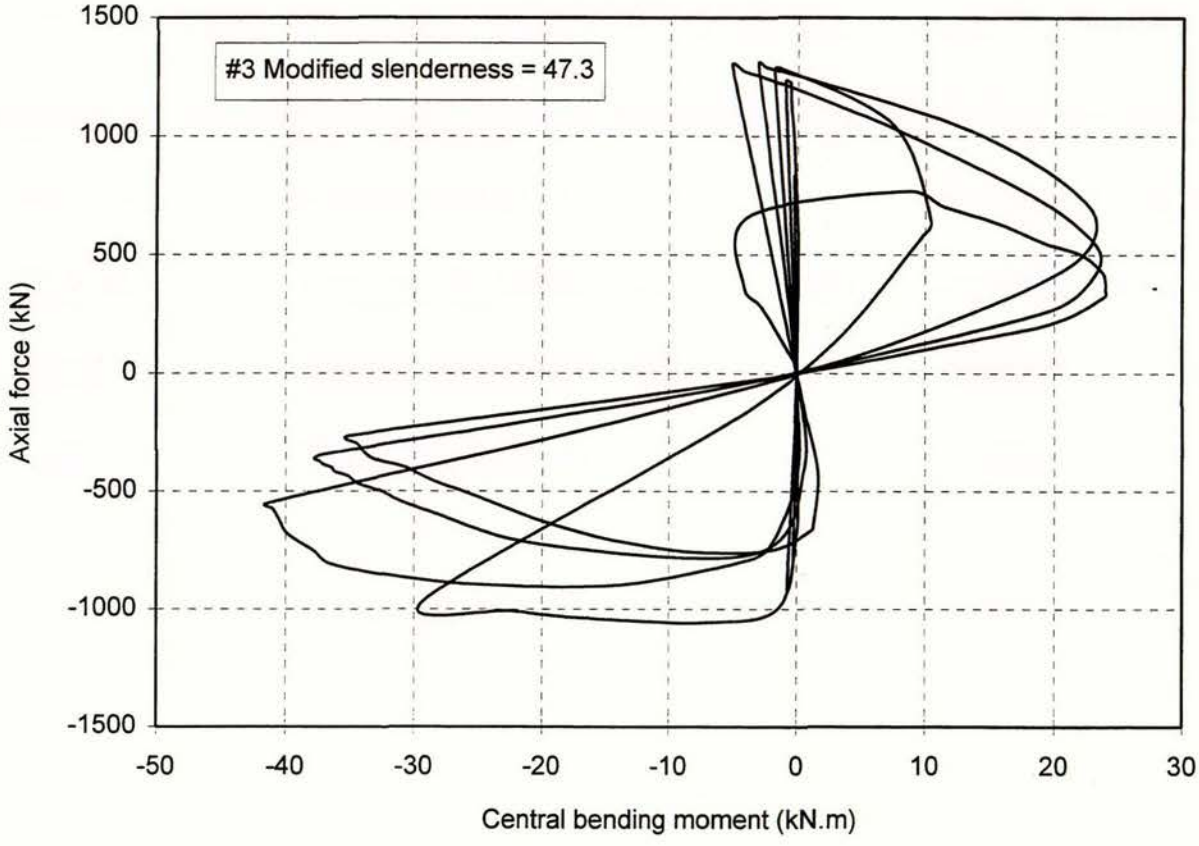

Figure 3.6 Specimen #3: Test axial force versus central bending moment

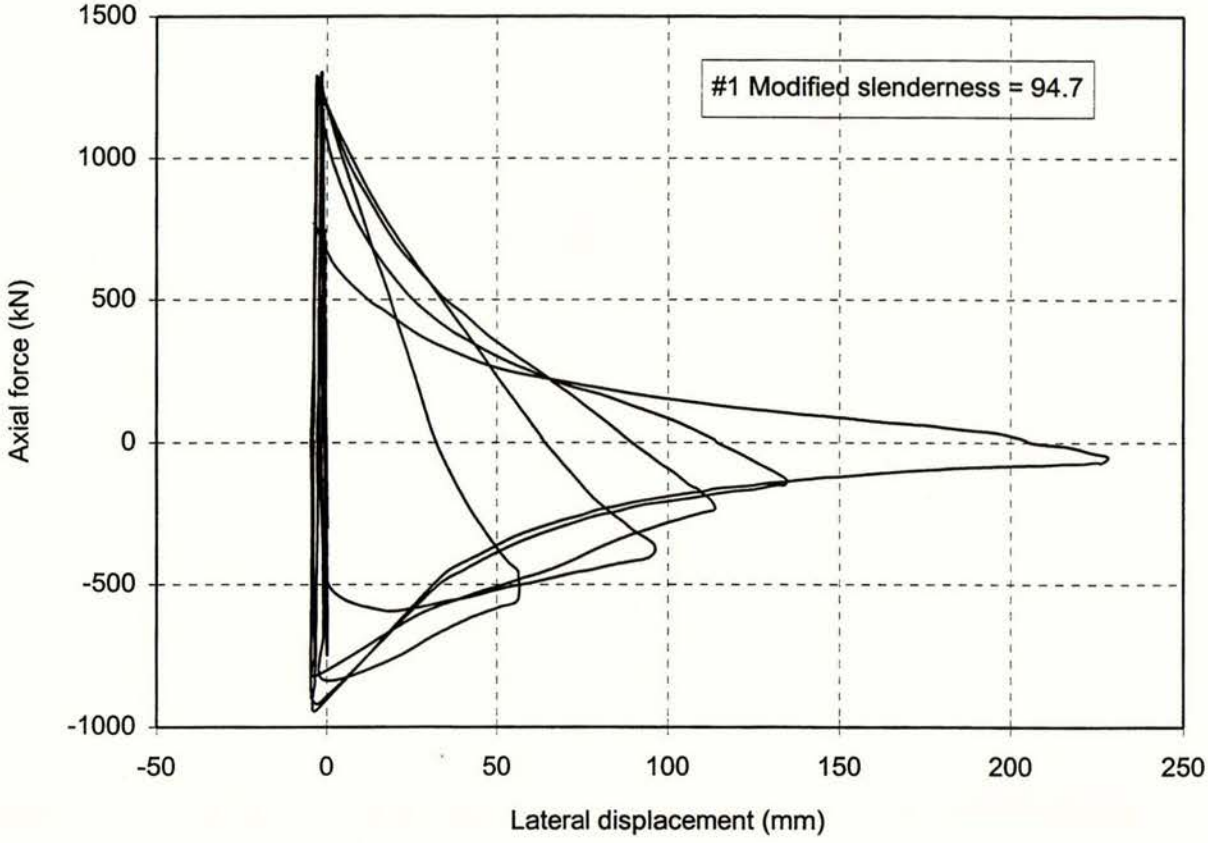

Figure 3.7 Specimen #1: Test axial force versus lateral displacement

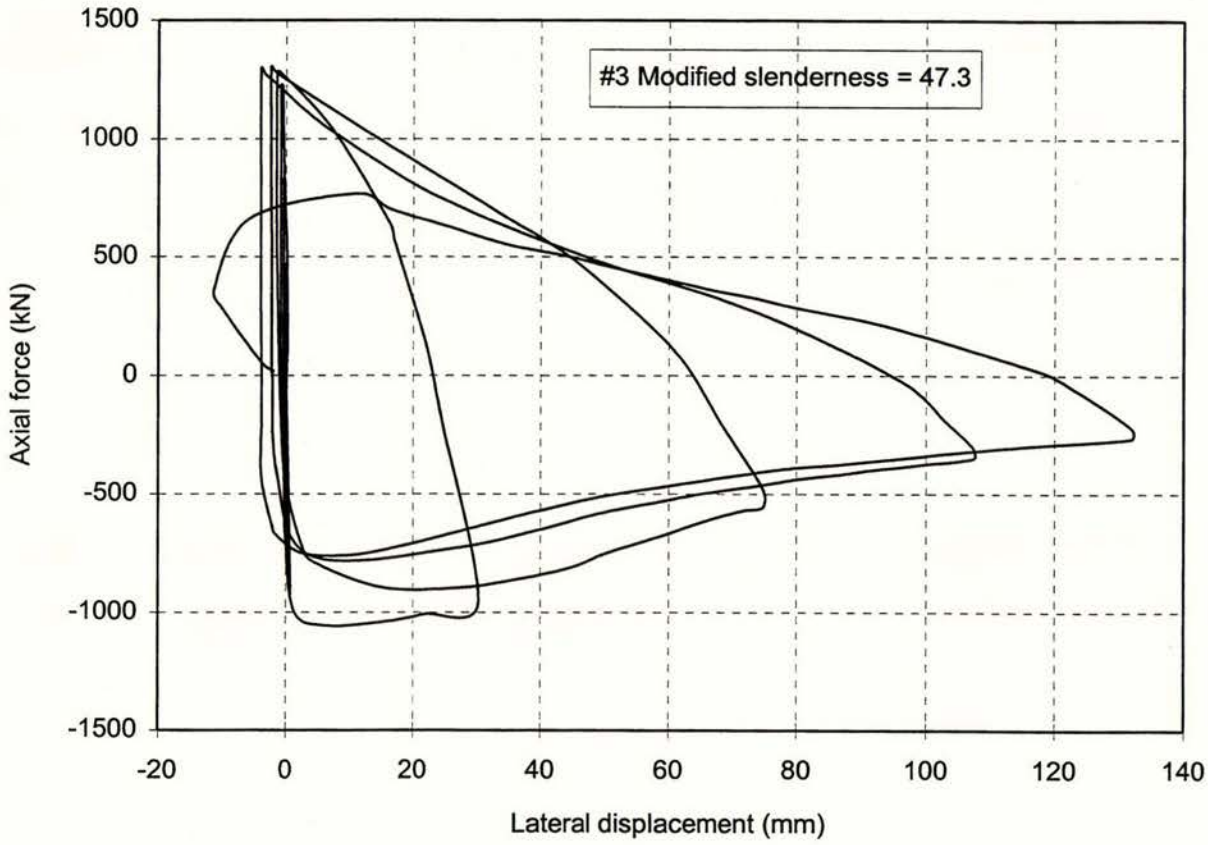

Figure 3.8 Specimen #3: Test axial force versus lateral displacement

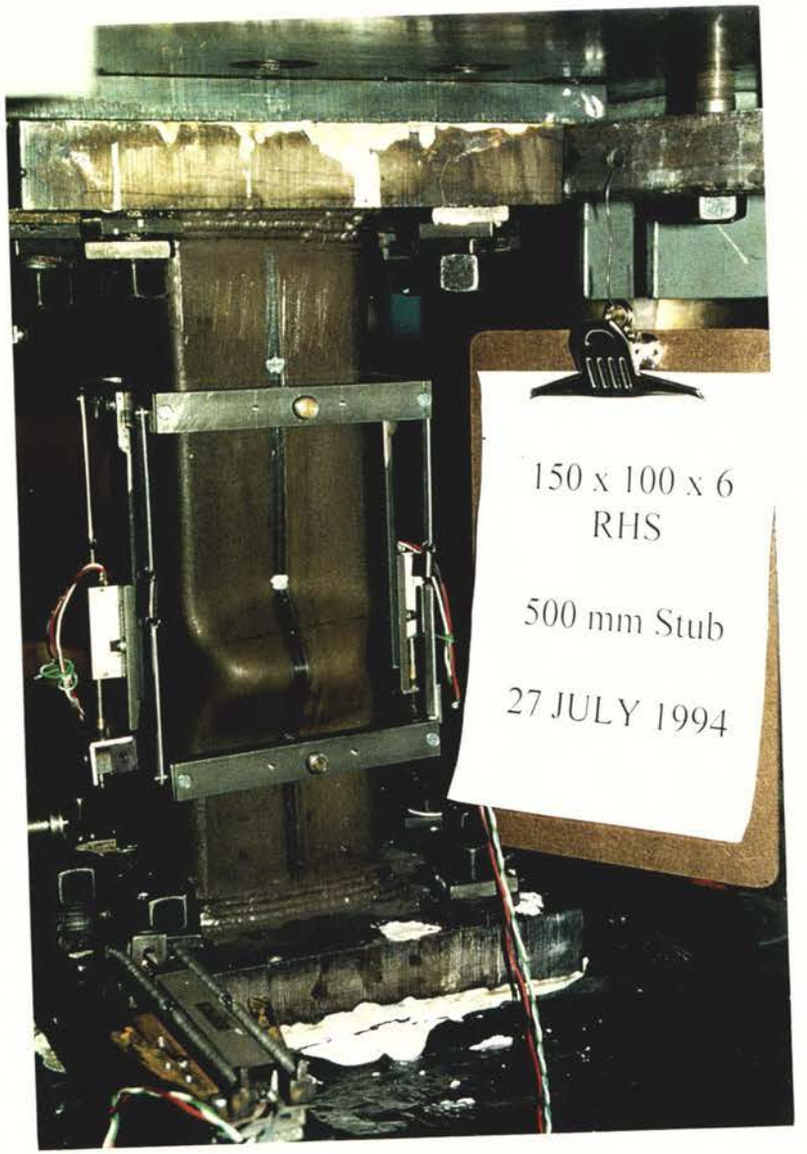

Figure 3.9 Stub column subjected to an axial contraction of 13.4 mm, with local buckling occurring

Figure 3.10 Specimen #1 subjected to a contraction of 19.4mm, showing overall buckling and local buckling

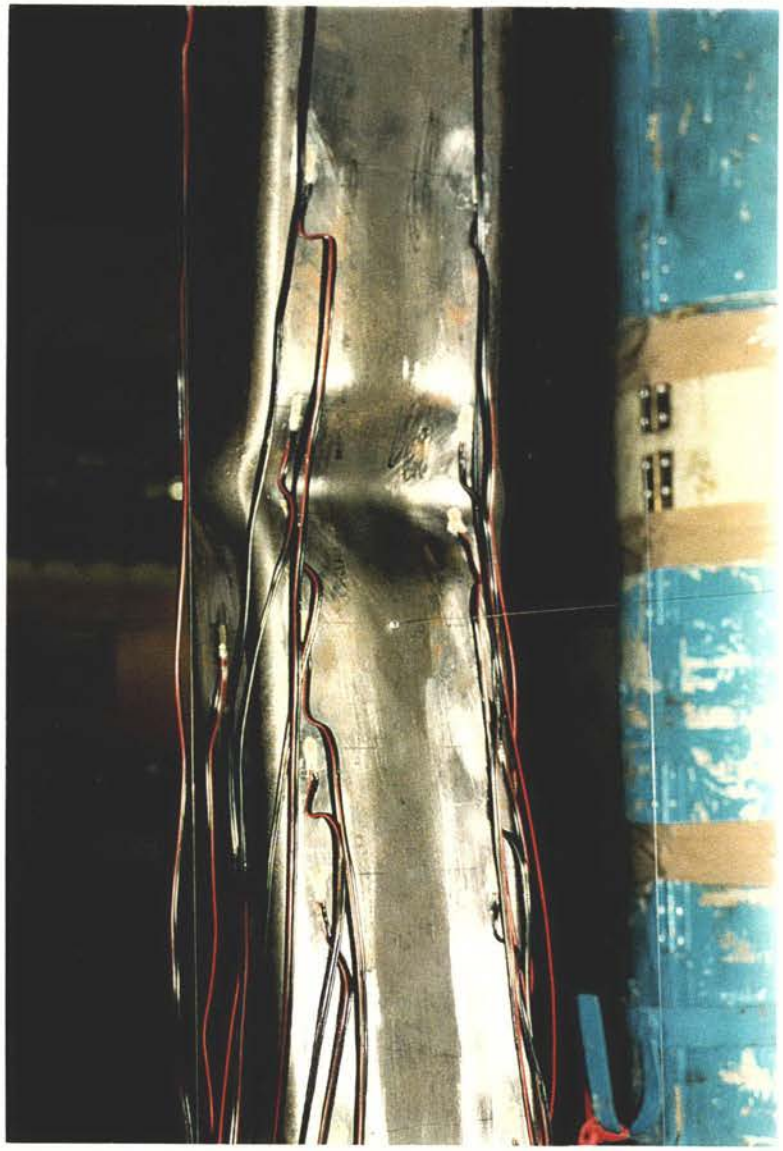

Figure 3.11 Specimen #1 showing the local buckle in cycle 6 at ductility 4.2

Figure 3.12: Specimen #1 subjected to a contraction of -39.6 mm, axial ductility of -8.56 in the seventh cycle. Overall and local buckling are evident.

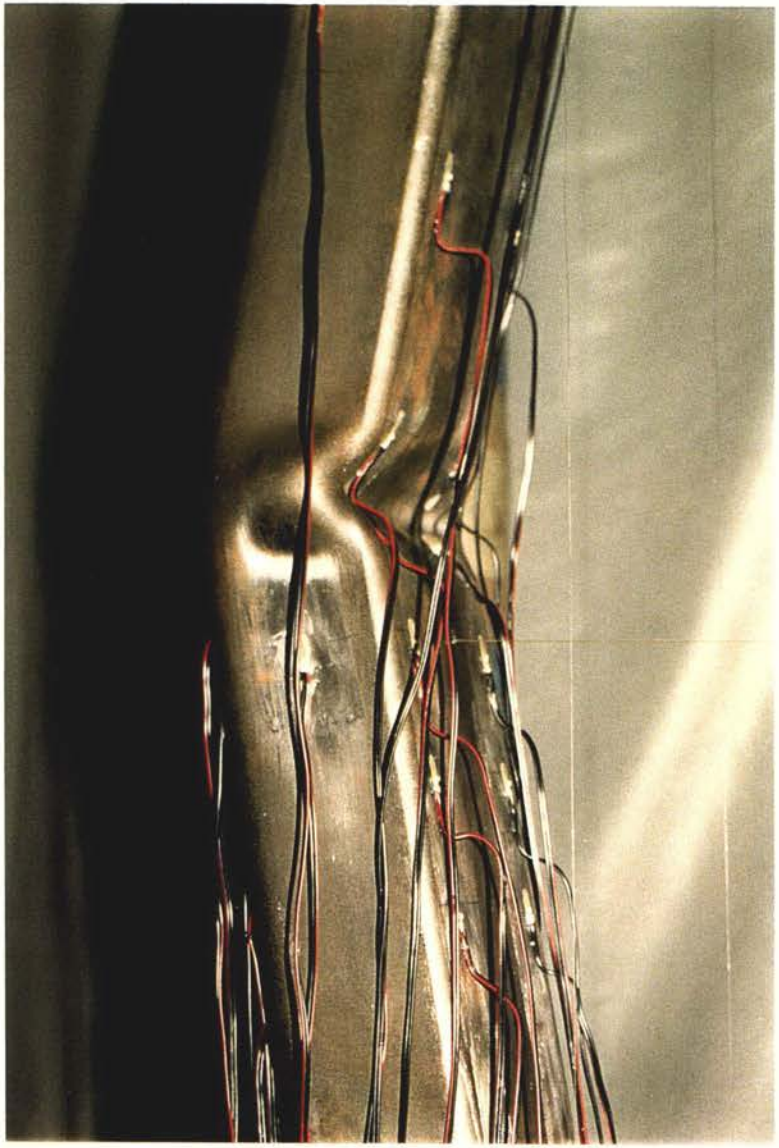

Figure 3.13: Specimen #1,View of the local buckle shown in figure 3.12

Figure 3.14: Specimen #1 at the end of the test showing the fracture on one side of the member at mid-height.

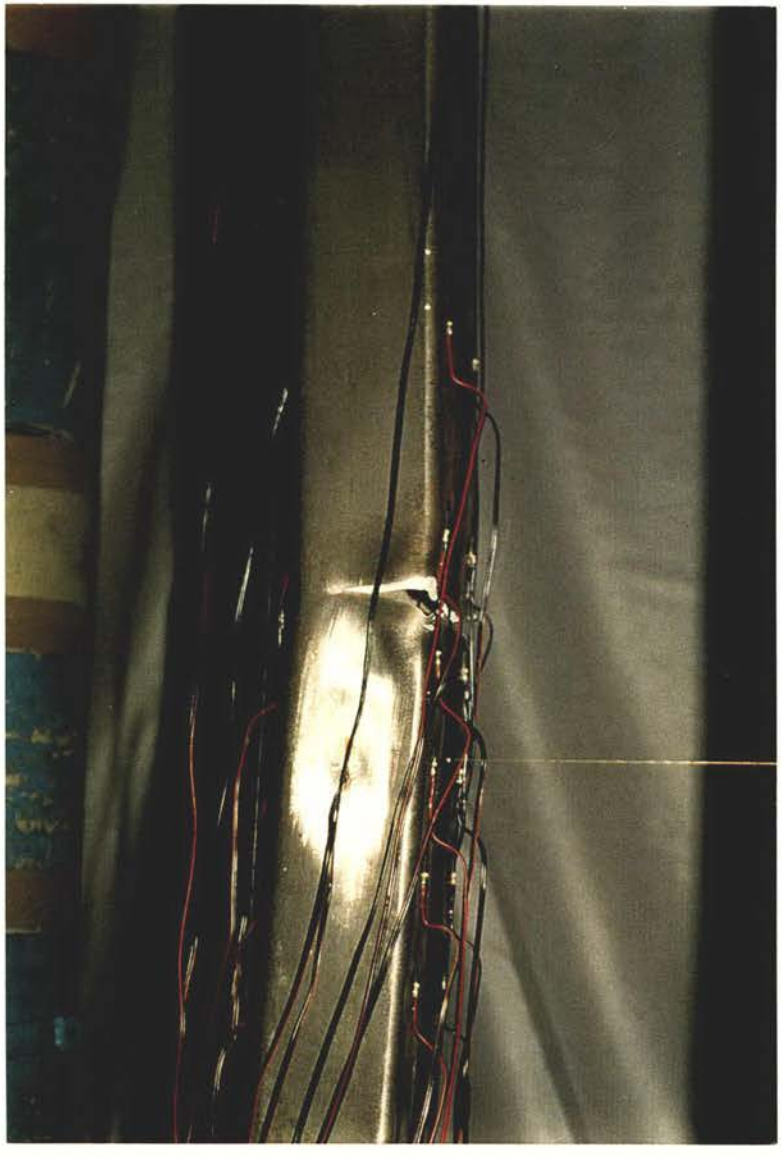

Figure 3.15 Specimen #1: view of the fracture at the end of the test.

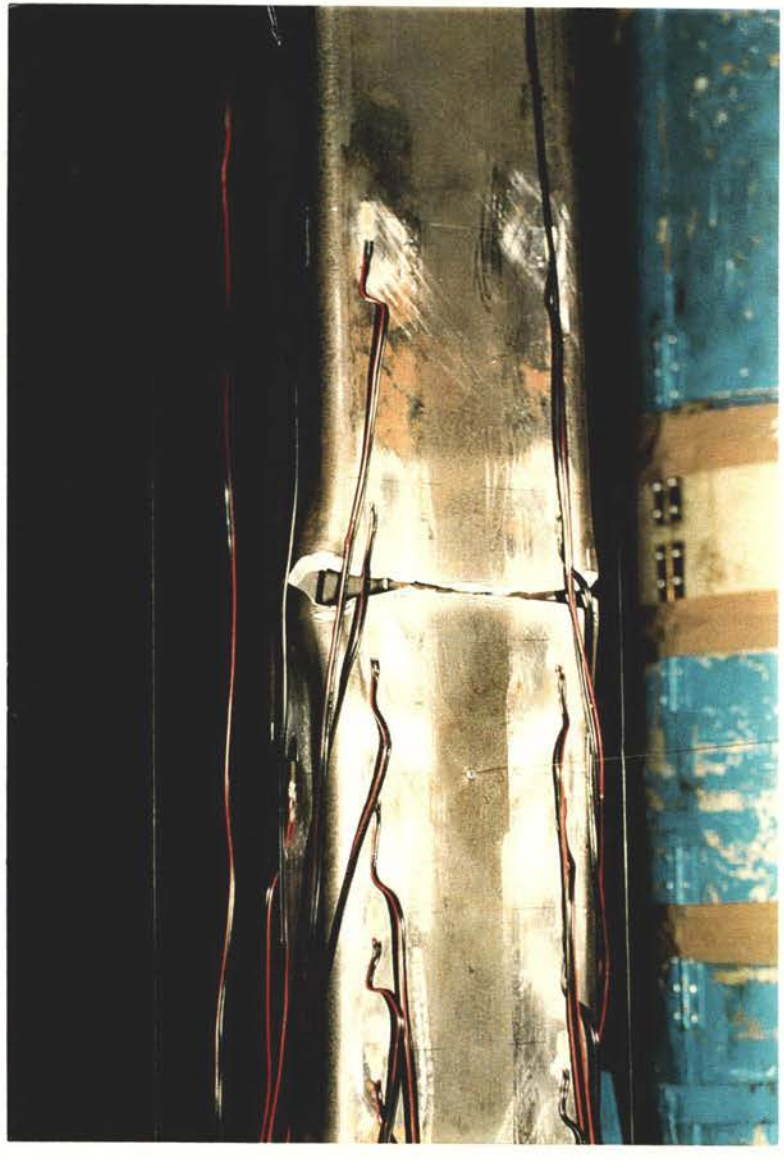

Figure 3.16 Specimen #1: view of the fracture at the end of the test.

Figure 3.17 Specimen #2 in cycle 7 showing overall and local buckling

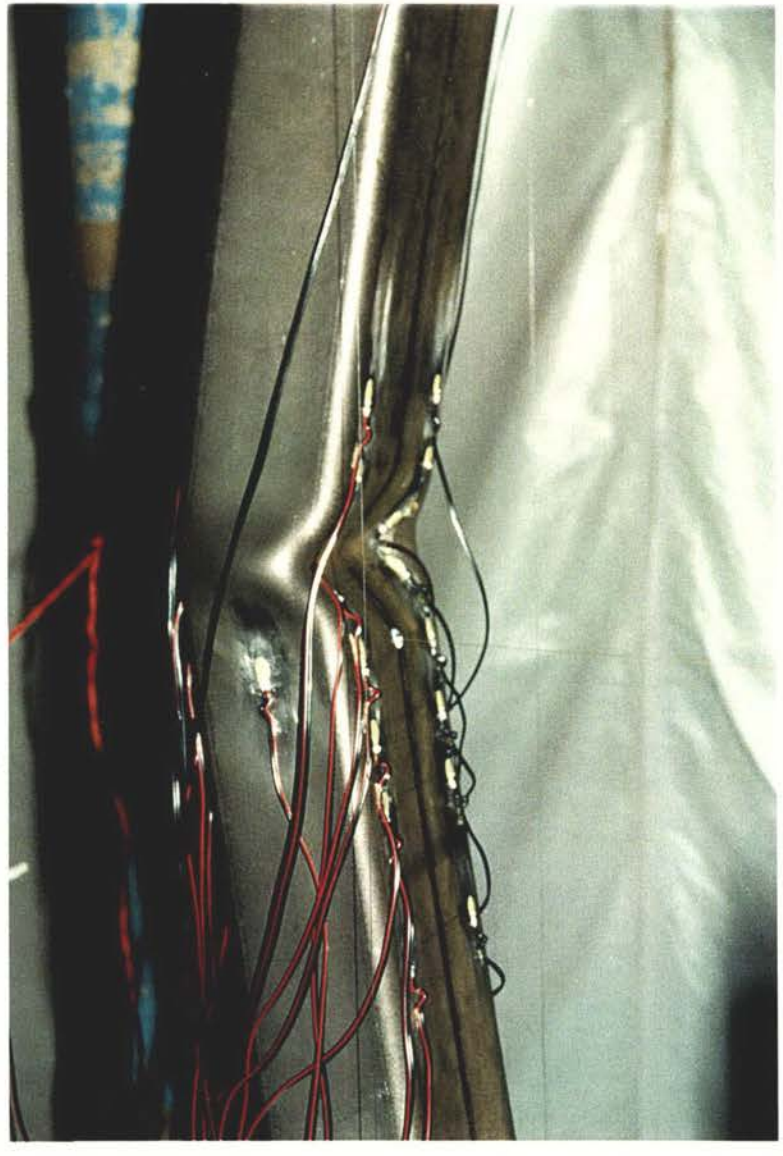

Figure 3.18 Specimen #2: Local buckle shown in figure 3.17

Figure 3.19 Specimen #2 at the end of the test

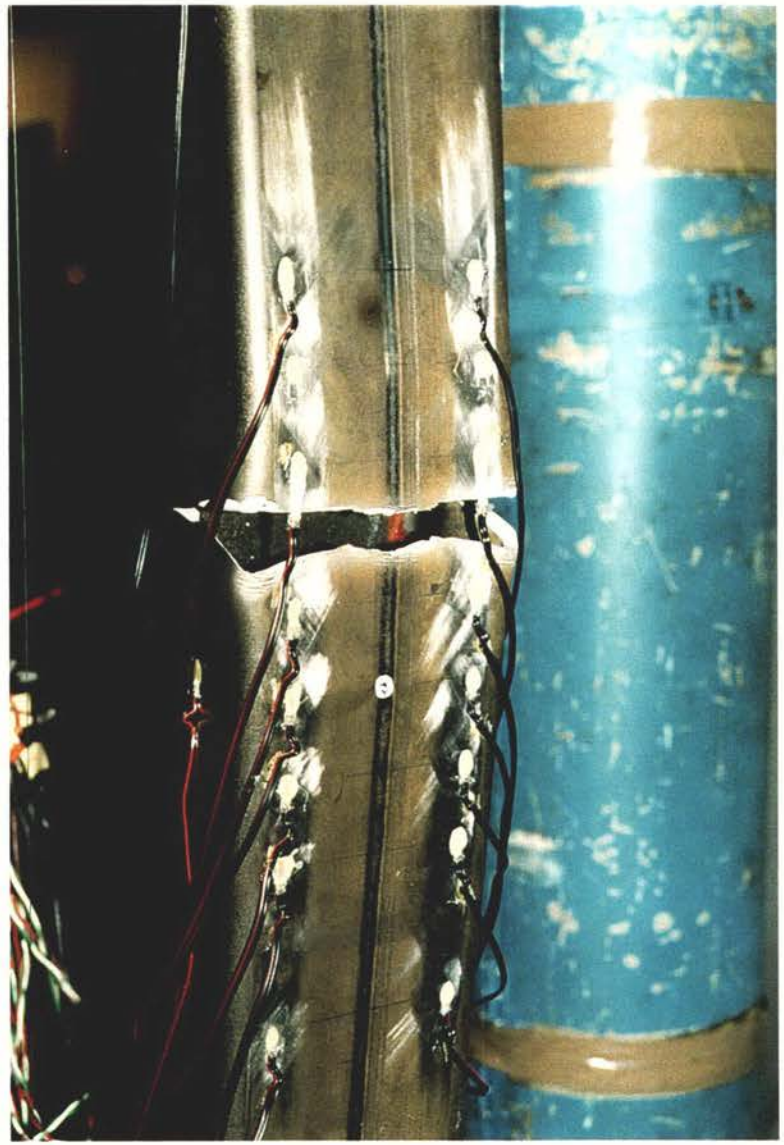

Figure3.20 Specimen #2 Fracture at the mid-height at the end of the test

Figure 3.21 Specimen #3 in cycle 5 showing overall and local buckling

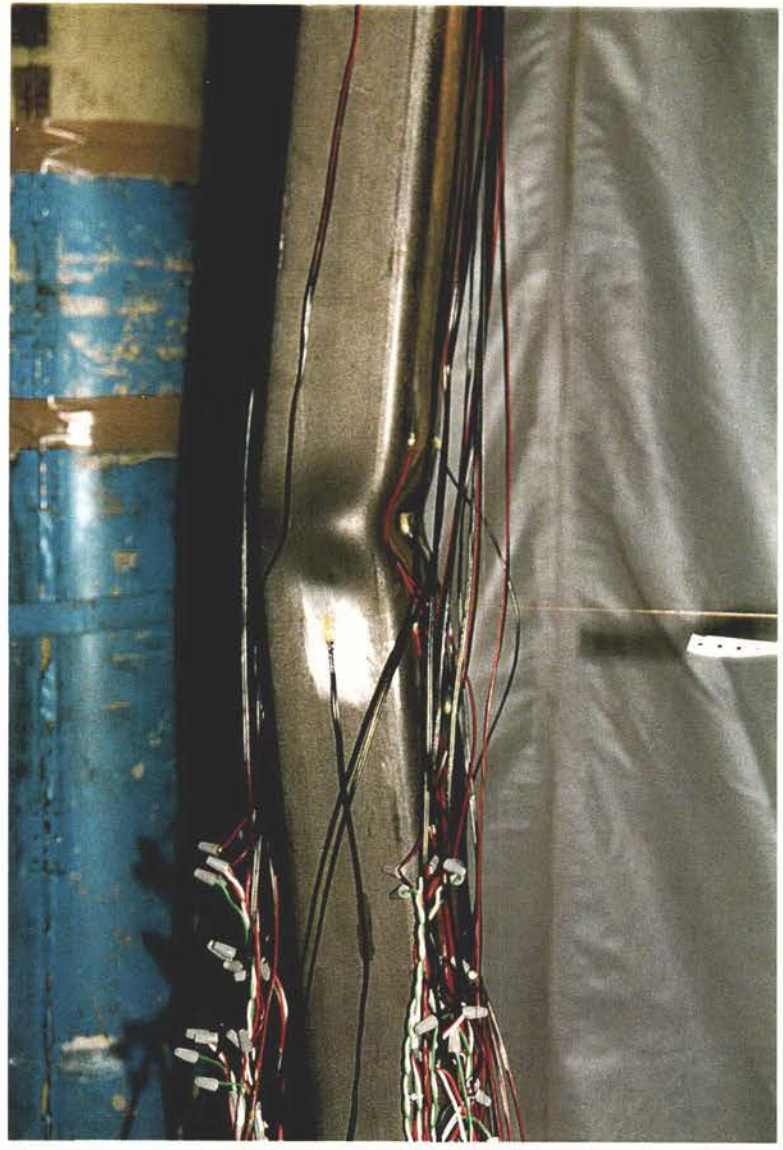

Figure 3.22 Specimen #3 showing the local buckle seen in figure 3.21

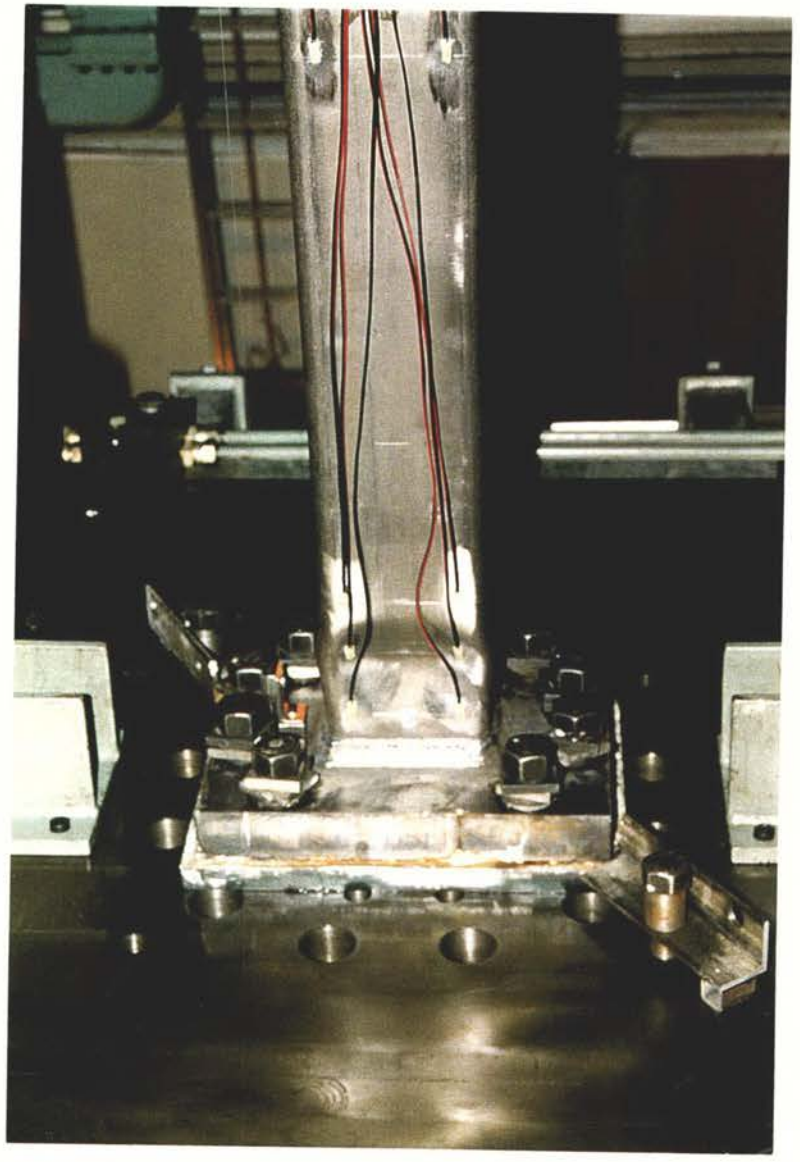

Figure 3.23 Specimen #3 Local buckle at the fixed end of the member

Figure 3.24 Specimen #3 in cycle 7 near the end of the test, showing a crack at the mid-height of the member

CHAPTER 4

THEORETICAL MODELLING

Typical member geometry is shown in Figure 4.1(a). The member is loaded with the axial force P, which causes the internal moment M, the axial deformation δ, the lateral deformation Δ and the plastic rotation θ. Plastic action is assumed to be concentrated in the central plastic hinge. The half-members, on either side of the plastic hinge region, are assumed to be subjected only to elastic actions.

Figure 4.2 illustrates the behaviour of a steel member when subjected to compression and tension loads. The basic curves for axial load P versus axial deformation δ, plastic hinge rotation θ and the moment at mid-span M are shown in Figure 4.2, together with an indication of the physical behaviour in each zone. Figure 4.2 illustrates the behaviour of a typical member loaded in compression, where after elastic shortening, buckling takes place, followed by plastic action in the hinge region with the P-M curve limiting the strength of the interaction between axial load P and moment M. When the load reverses direction, elastic elongation occurs until the limit of the P-M interaction strength curve is reached, when plastic action in tension takes place in the hinge region. This is followed by yielding through the length of the member in tension until the load is reversed, when elastic shortening in tension occurs. The axial displacement is made up of the following components: elastic shortening, geometric shortening, displacement in the plastic hinge, yielding in tension and residual displacement, caused by material non-linearities.

Theoretical and phenomenological models for brace members have been developed previously. The refined physical model was developed by Ikeda and Mahin [5, 6] and combines both the aforementioned models. An idealised relationship between the tangent modulus and stress can be developed, from the stress-strain curve measured in a stub column test. The tangent modulus can be defined as a function of the axial force and the direction of the axial load increment, as shown in Figure 4.1(b). The limiting strength under the combined axial force and moment was based on a

single continuous function. The development of this function by Remennikov and Walpole is explained in reference [7]. The equation while lacking physical significance, conforms closely to a realistic, physically-derived surface, which is continuous and convex and is suitable for computer implementation. The equation was developed for 150 UC 30 rolled steel members. It was found to give theoretical curves which were close to the test curves for the RHS sections in this research. Further research may allow the development of an interaction equation specifically for RHS members. This could give better agreement between theory and test. The interaction equation used for axial load p and bending moment m_y applied about the minor axis, is given below.

$$p^2 + m_y^4 + 3.68p^6m_y^2 + 10.4p^6m_y^4 = 1$$

The Ikeda model features a gradual transition from the elastic shortening zone ES2 to the plastic zone in compression P1 and represents the degradation of strength that occurs in the plastic zone in compression P2, after a gradual transition from elastic elongation in tension EL2. Figure 4.4 shows the theoretical variation of plastic rotation with axial load. The plastic axial and rotational deformations at the plastic hinge are based on the plastic flow rules. Several behavioural characteristics are included in the model to achieve better representation of the observed behaviour. These empirical characteristics, include the variation of the tangent modulus during cycles, the gradual plasticification process of the plastic hinge and the residual displacement, caused by material non-linearities in the nominal elastic range. The tangent modulus of elasticity is employed in place of the initial modulus of elasticity, to allow for material non-linearities. The degradation of the tangent modulus of elasticity from cycle to cycle is ignored. The effective length is used in place of the actual length for determining buckling characteristics.

The theoretical curves can be calculated from the physical model and the imposed displacements. The brace routine developed by Remennikov and Walpole [7] was used. The input data included the imposed displacements listed earlier in Table 2.4. The input data for the three specimens is listed in Appendix 1.

Table 4.1 shows the values of e1, e2, e3, and e4 etc assumed.

Table 4.1

e1	e2	e3	e4
0.05	0.9	1.2	0.0

Figures 4.3, 4.4 and 4.5 show the theoretical variation of the axial force with axial displacement for the specimens #1, #2 and #3 respectively.

Figures 4.6 to 4.8 show the theoretical variation of axial force with the bending moment at the mid-height of the member for the specimens #1, #2 and #3 respectively.

Figure 4.9 to 4.11 shows the theoretical variation of axial force with lateral force for the specimens #1, #2 and #3 respectively.

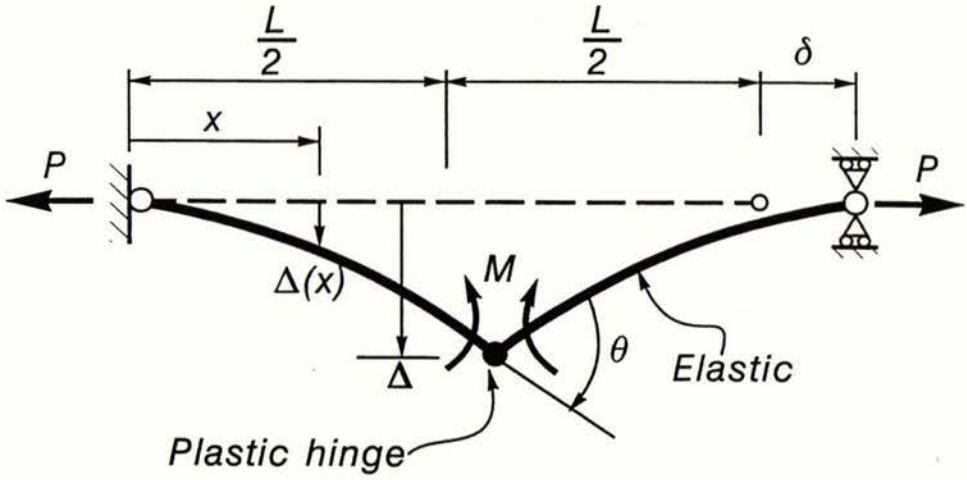

Figure 4.1(a) Member Geometry

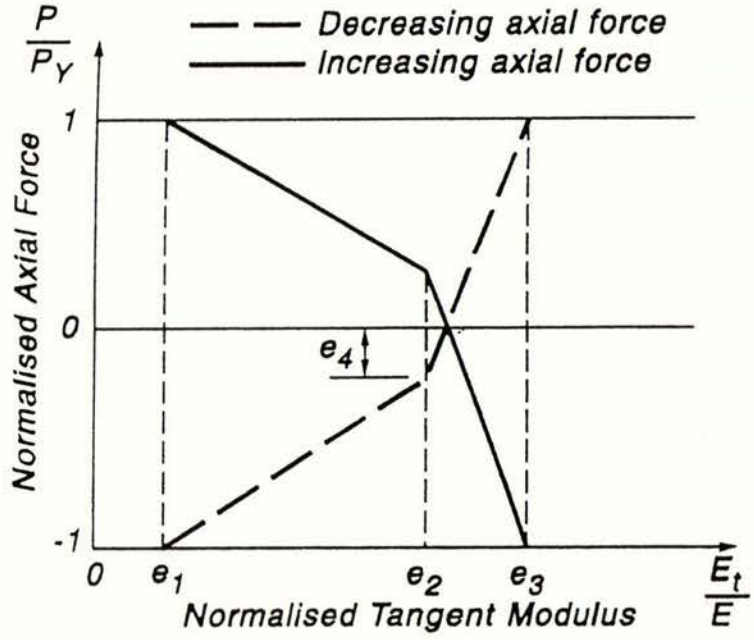

Figure 4.1(b) Axial force versus tangent modulus

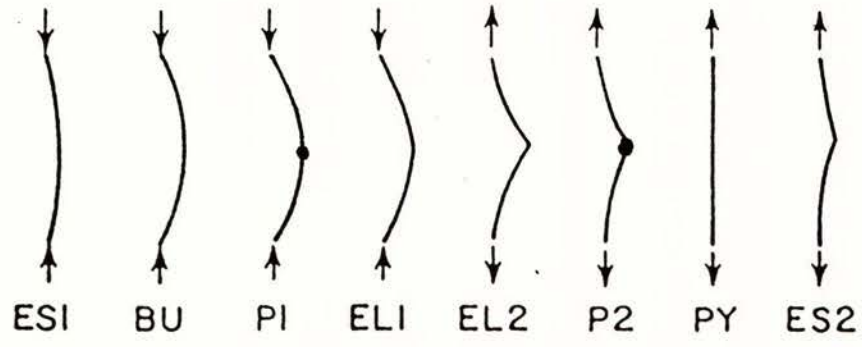

ES1 = Elastic shortening zone in compression
BU = Buckling Zone
P1 = Plastic Zone in compression
EL1 = Elastic elongation zone in compression
EL2 = Elastic elongation zone in tension
P2 = Plastic zone in tension
PY = Yielding zone
ES2 = Elastic shortening zone in tension

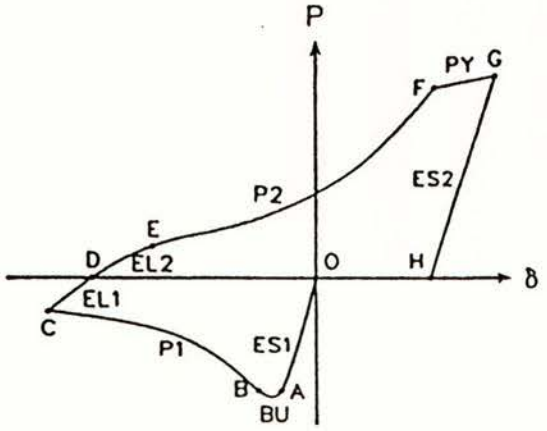

(a) P - δ Curve

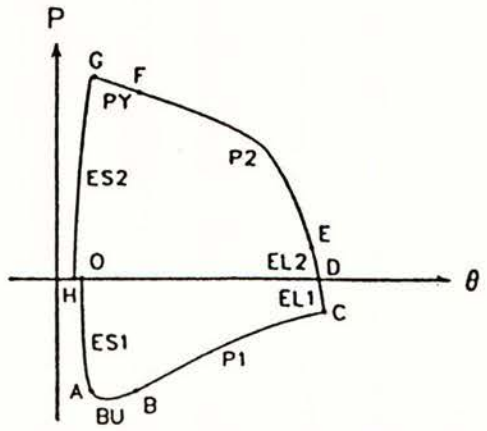

(b) P - θ Curve

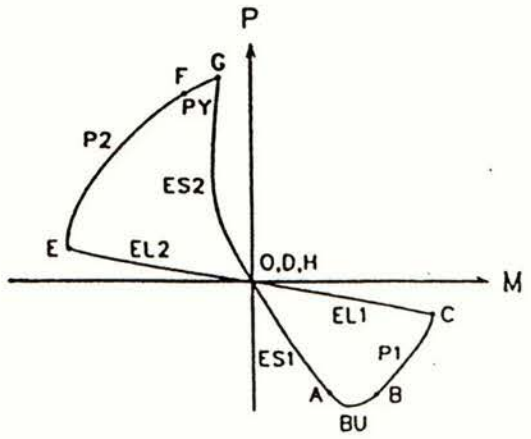

(c) P - M Curve

Figure 4.2 Behaviour of a steel brace member

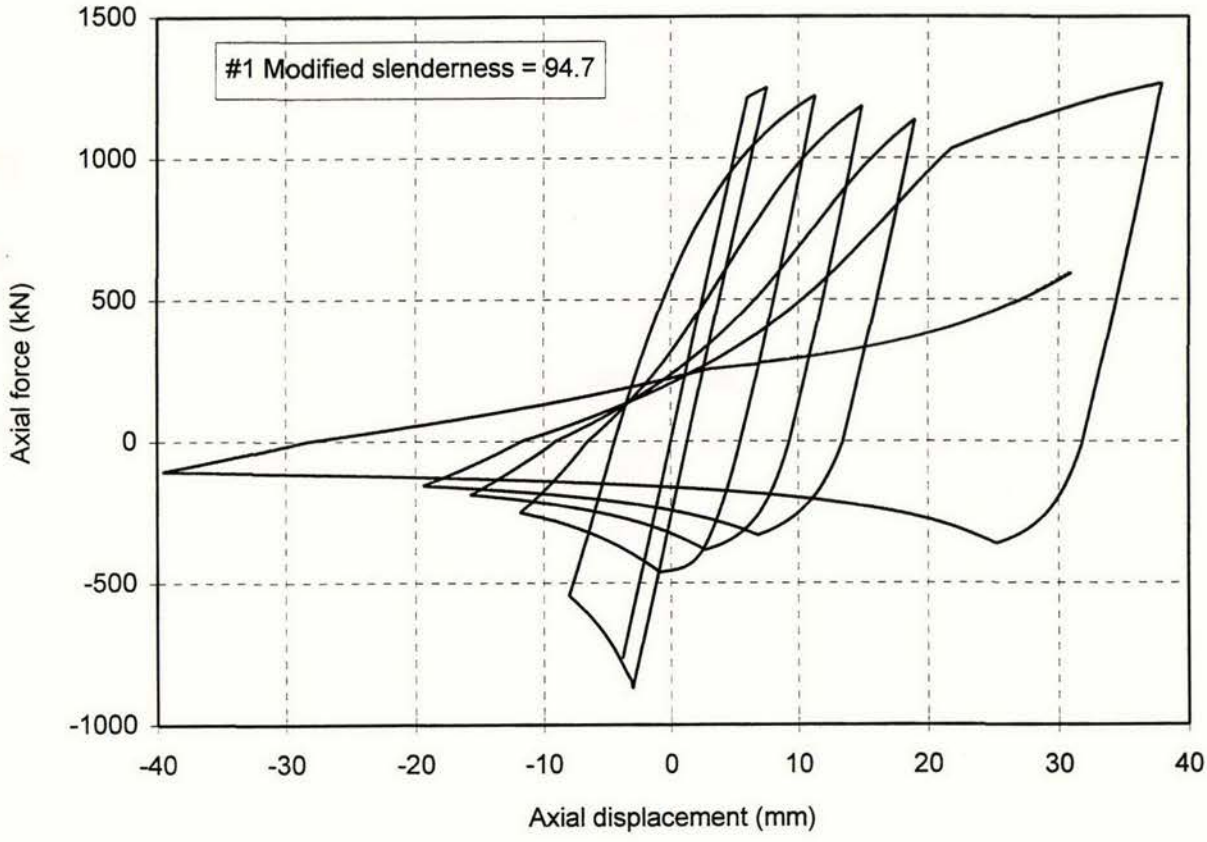

Figure 4.3 Specimen #1: Theoretical axial force versus axial displacement

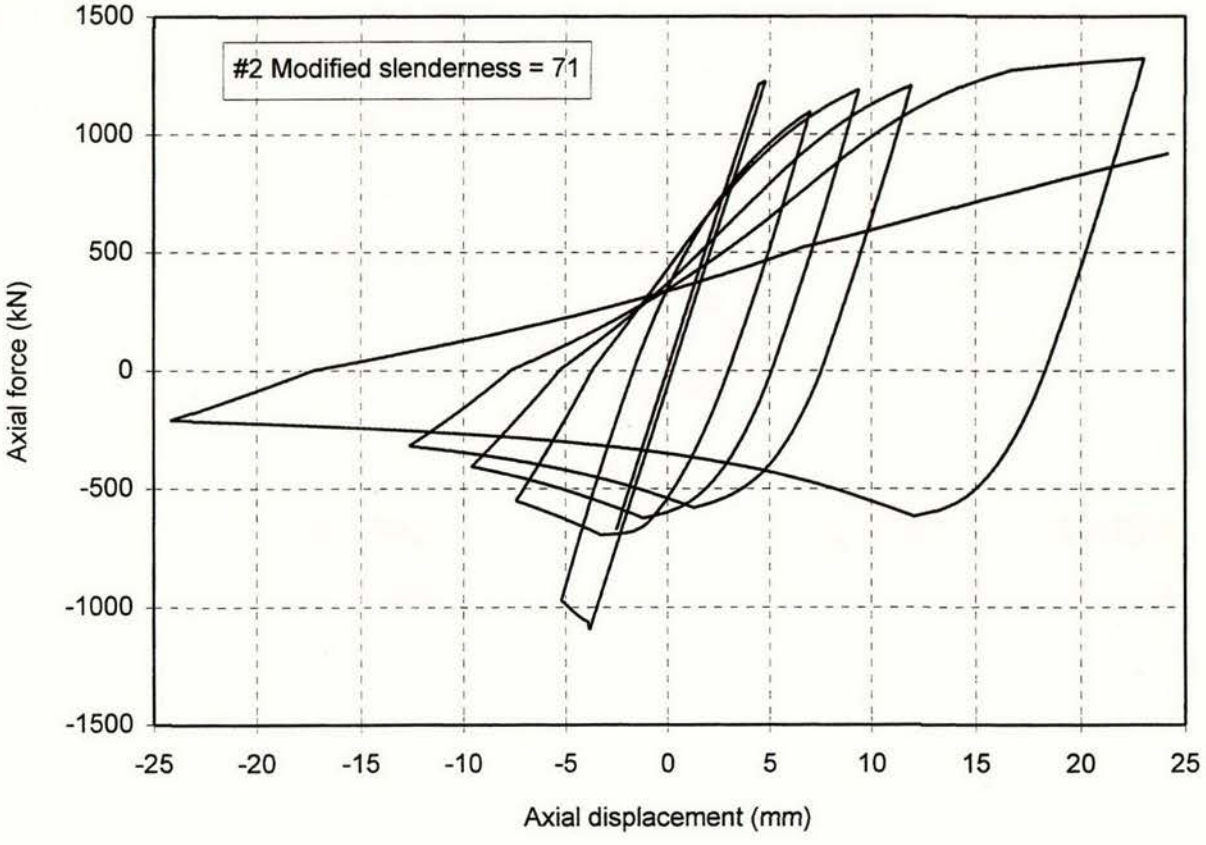

Figure 4.4 Specimen #2: Theoretical axial force versus axial displacement

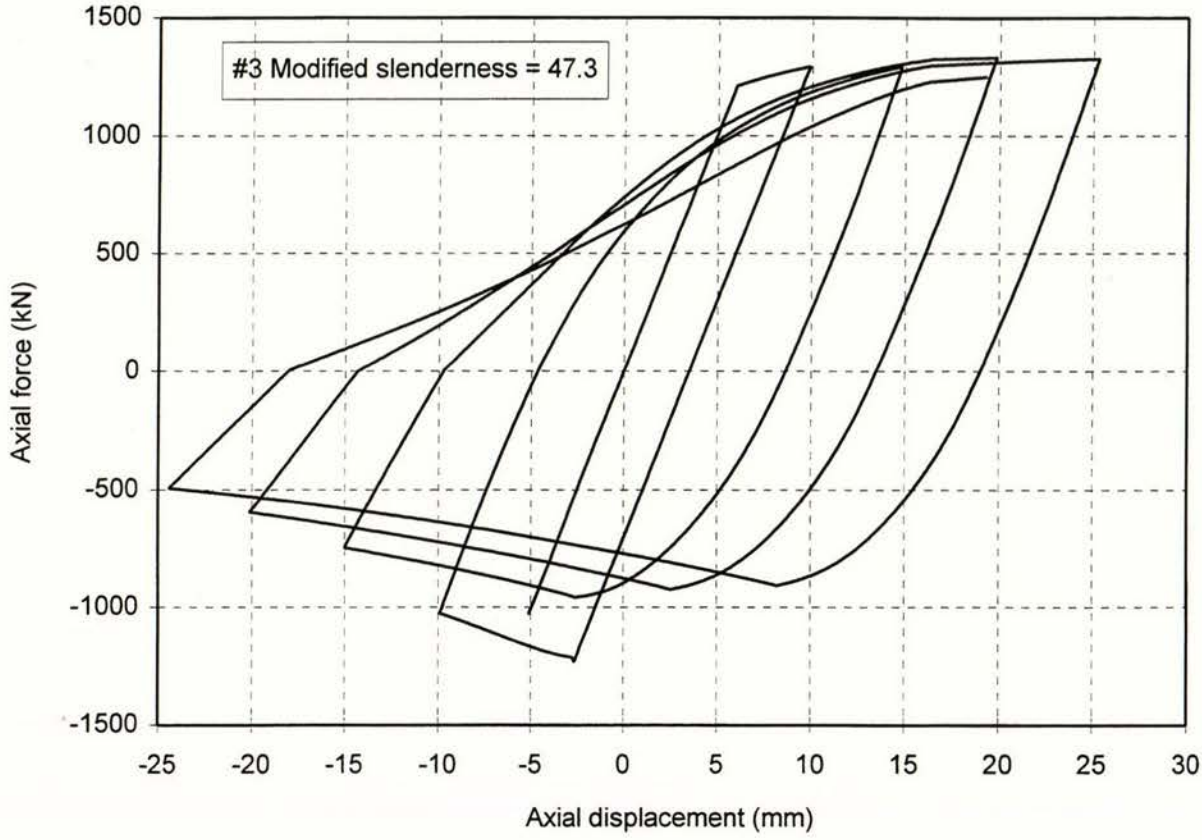

Figure 4.5 Specimen #3: Theoretical axial force versus axial displacement

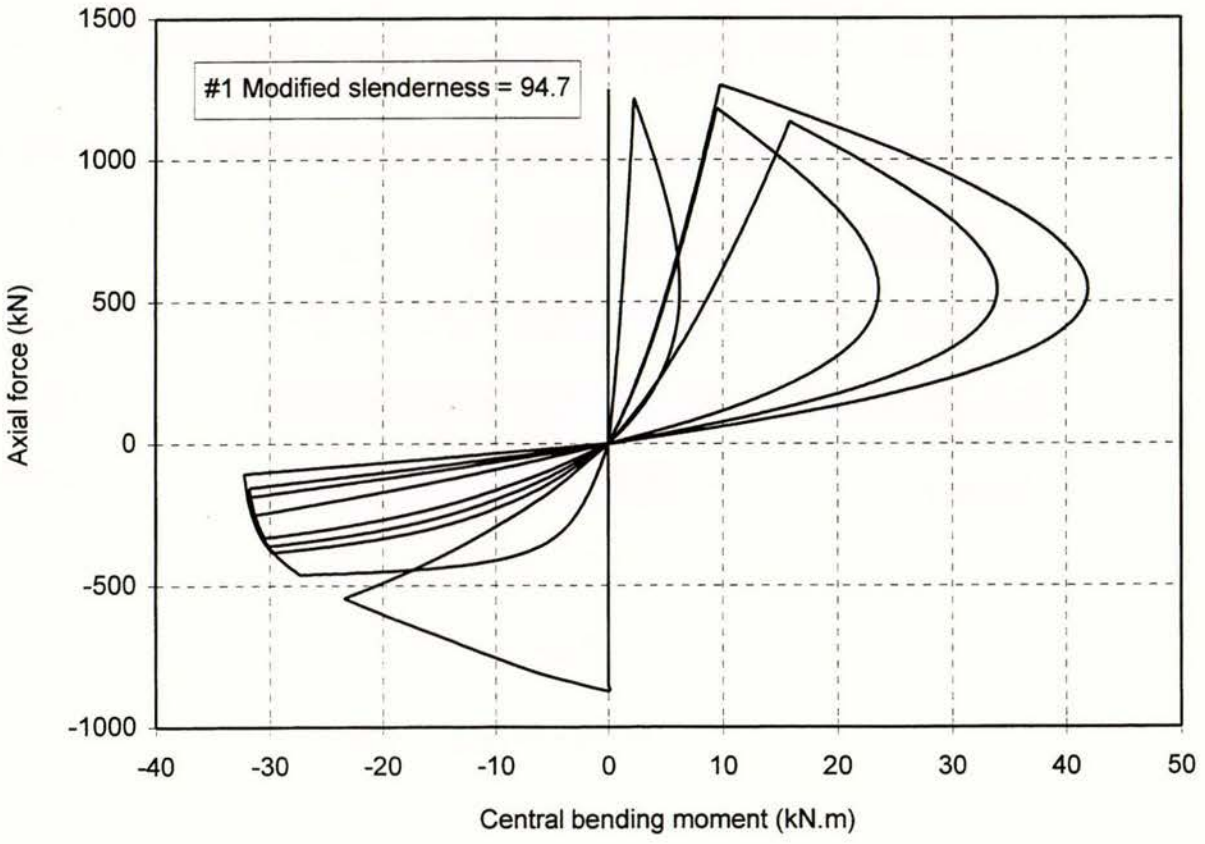

Figure 4.6 Specimen #1: Theoretical axial force versus central moment

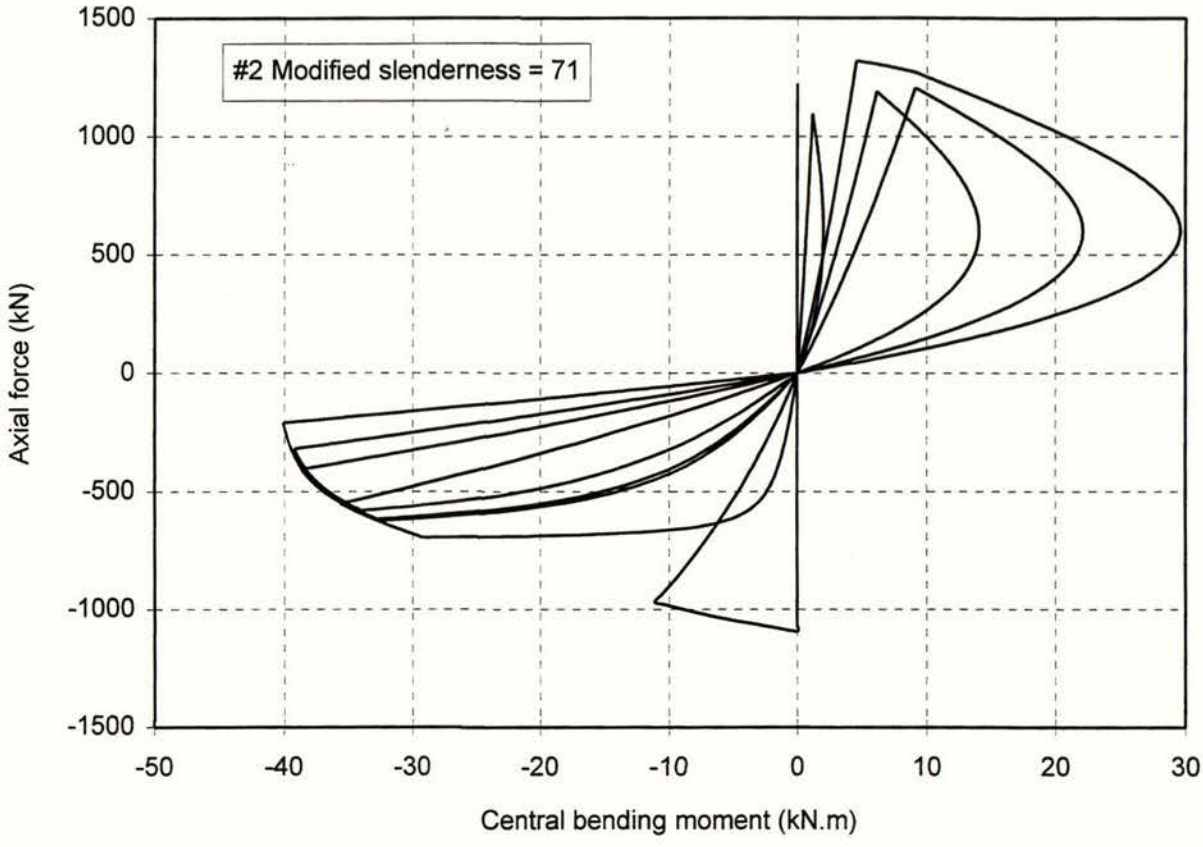

Figure 4.7 Specimen #2: Theoretical axial force versus central moment

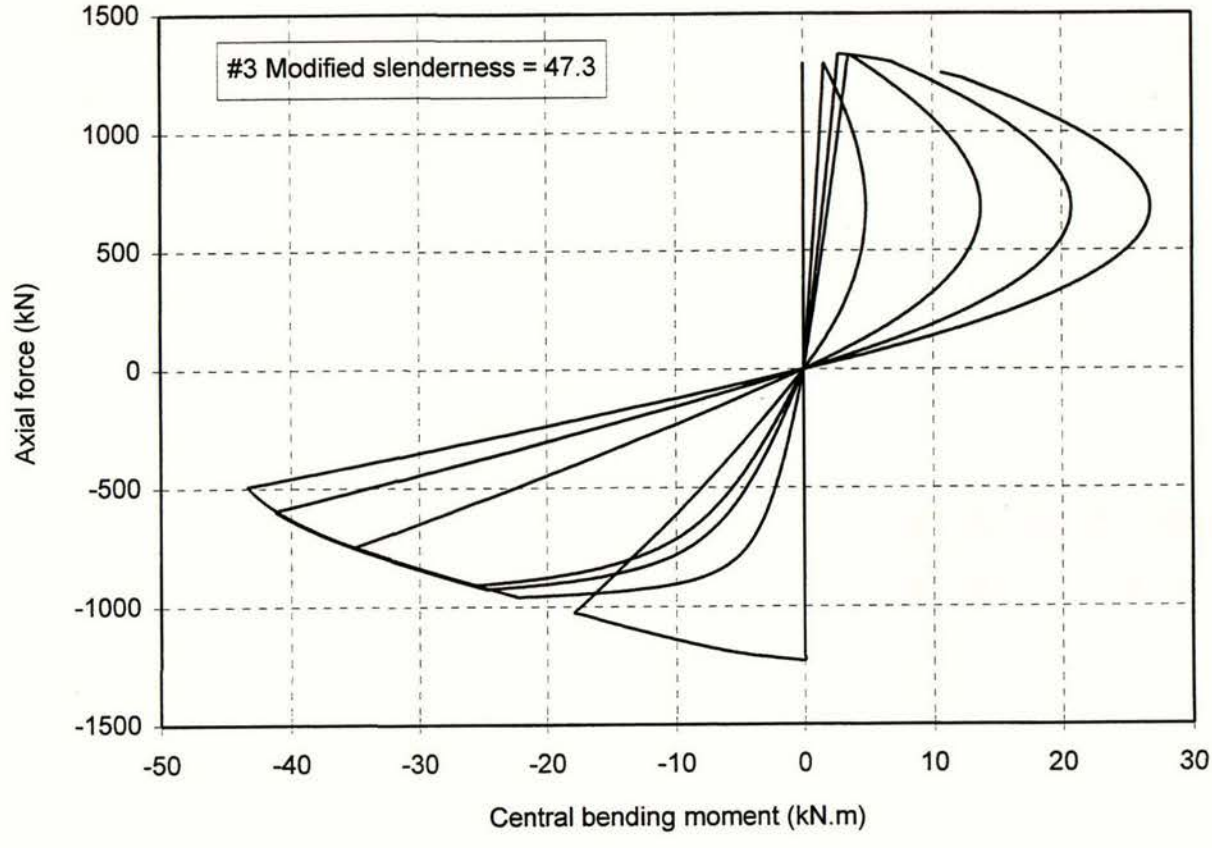

Figure 4.8 Specimen #3: Theoretical axial force versus central bending moment

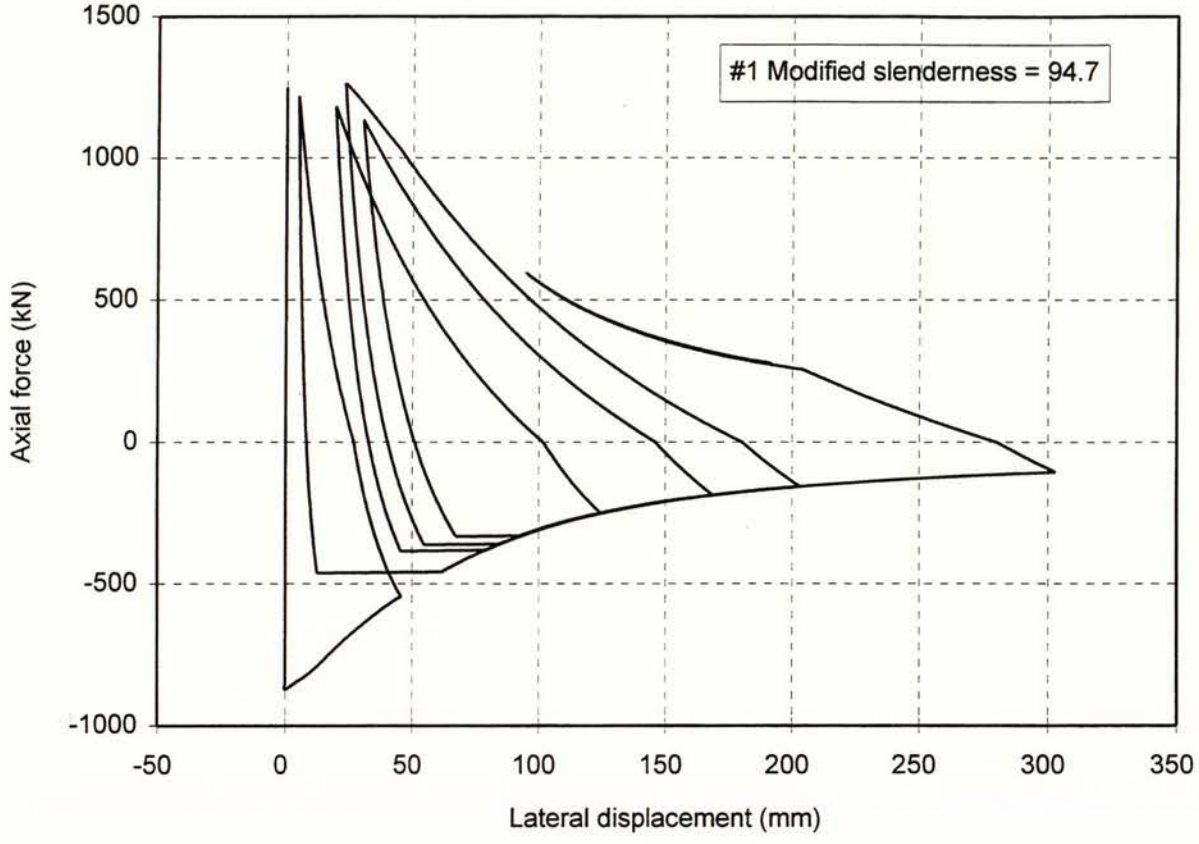

Figure 4.9 Specimen #1: Theoretical axial force versus lateral displacement

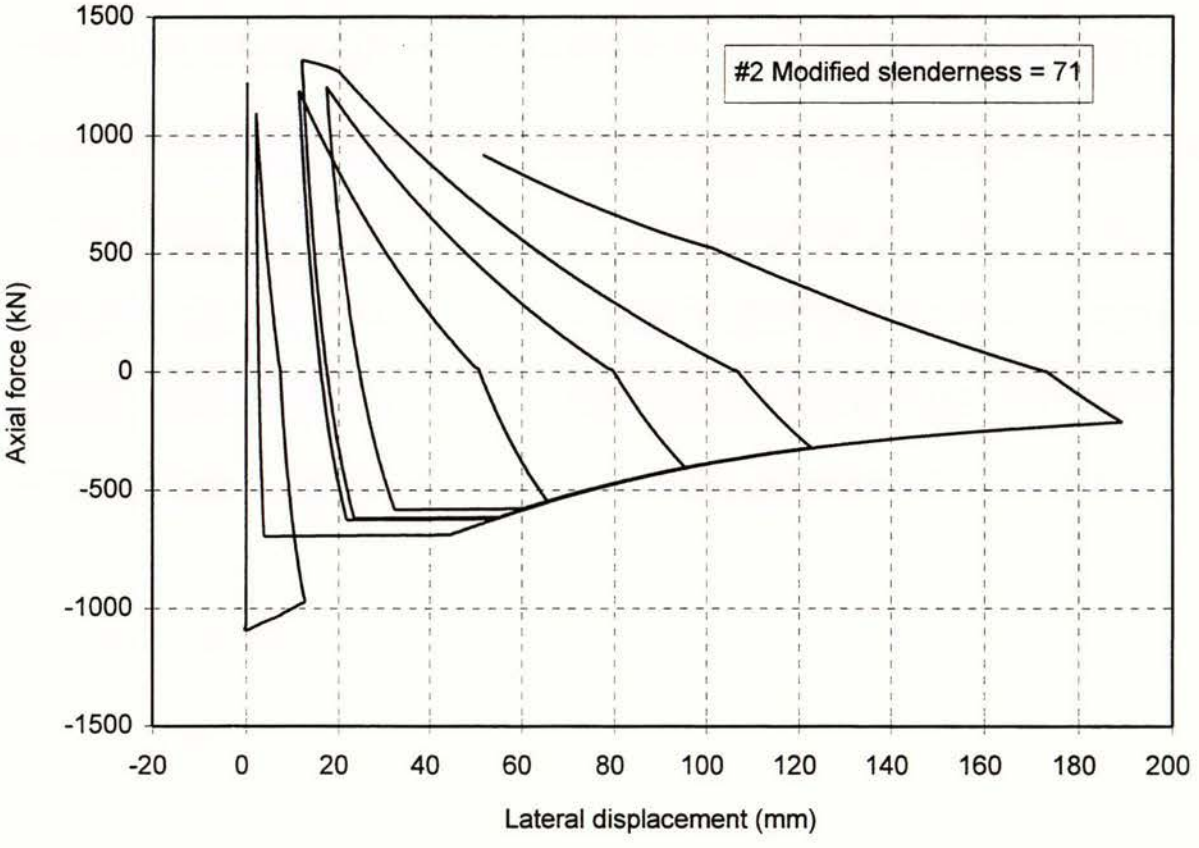

Figure 4.10 Specimen #2: Theoretical axial force versus lateral displacement

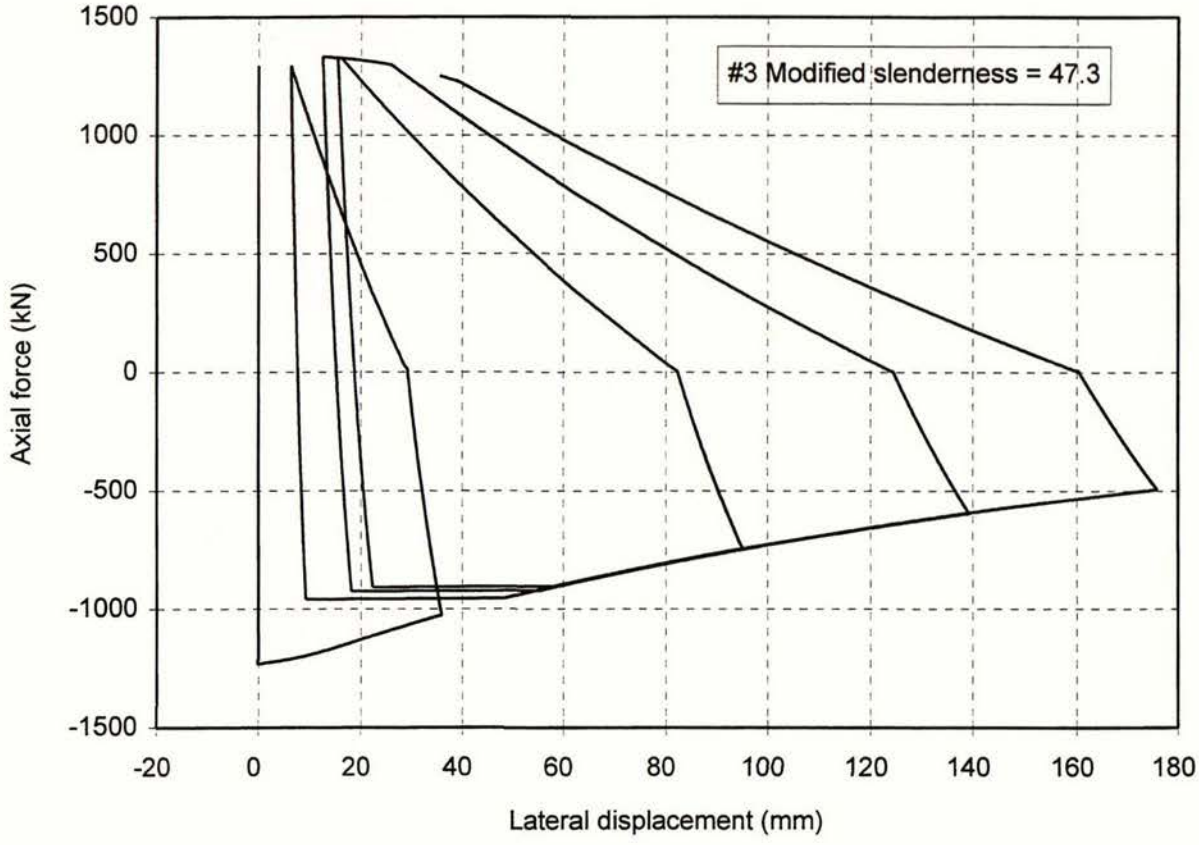

Figure 4.11 Specimen #3: Theoretical axial force versus lateral displacement

CHAPTER 5

COMPARISON OF TESTS AND THEORY

Figure 5.1 compares how the axial force varied with the axial displacement in the test for specimen #1 with that predicted by the theoretical brace routine. Generally the agreement is very good with the shape and slopes of the curves being very similar. The magnitude of the first buckling load is accurately predicted and so is the magnitude of the second buckling load. The magnitudes of the remaining test buckling loads exceed those predicted by the theory. The recorded test load did not appear to vary in the way expected with a brace member. The magnitude of each successive peak compressive load is expected to be less than the previous peak. This is comparing specimen #1 with others reported in the literature [8,9] and also with specimens #2 and #3, and with the Universal Column specimens tested by Leowardi [2]. It would appear then, that the theory is satisfactory and that the recorded test data is anomalous. It would be interesting to repeat this test with another similar specimen and see if similar behaviour is obtained or not. When the specimen #1 was tested, the theoretically-predicted curves were not available. The first four theoretical peaks in the tensile loading become progressively lower than the test peaks. Possibly this is caused by more strain hardening in the test specimen. The fifth tensile peak shows very good agreement between test and theory. The final half cycle before fracture shows reasonable agreement, considering the specimen had fractured through one side.

A comparison of the variation of the axial force with the axial displacement in the test with that predicted with the theory for specimen #2 is shown in figure 5.2. Again the slopes and shape of the curves are very similar. The first buckling load was predicted accurately, the second, third, fourth and fifth predictions were slightly below the test loads. The predicted curves generally followed the shape of the test curves very well. The second, third and fourth theoretical maximum tensile loads were a little below the test loads. The fifth and final peak test tensile load was accurately predicted by the theory.

Figure 5.3 compares the variation of the axial force in the test with that predicted theoretically. There is very good agreement between the general shape and slope of the curves. The tensile peak values agree well between test and theory. The theoretical compressive peak values are all a small amount higher, than the test values. The test curves are more pinched after buckling than the theoretical curves.

Figure 5.4 compares the variation of the axial force with the central bending moment at the mid-height of specimen #1 for the test and theory. There is reasonable agreement in the compressive quadrant, but in the tensile quadrant the test curves have much smaller moment values than the theoretical curves.

The variation of the axial force with the central moment for specimen #3 is shown in figure 5.5 for the test and the theory. There is reasonable agreement in both the tensile and compressive quadrants.

The variation of the axial force with the lateral displacement is compared between theory and test in figure 5.6 for specimen #1. The theoretical curves have higher lateral displacements than the test curves. The curves are a similar shape to each other, but the agreement is only fair. This comparison is a severe test, because the theoretical lateral displacement must be derived from the theoretical plastic rotation, so there may be some accumulation of errors and approximations.

Similarly for specimen #3 in figure 5.7. The test and theory curves for #3 are similar to each other, but different in shape to the curves for #1. The theoretical curves are again larger than the test curves, but there is similarity between the shapes of the theoretical and test curves.

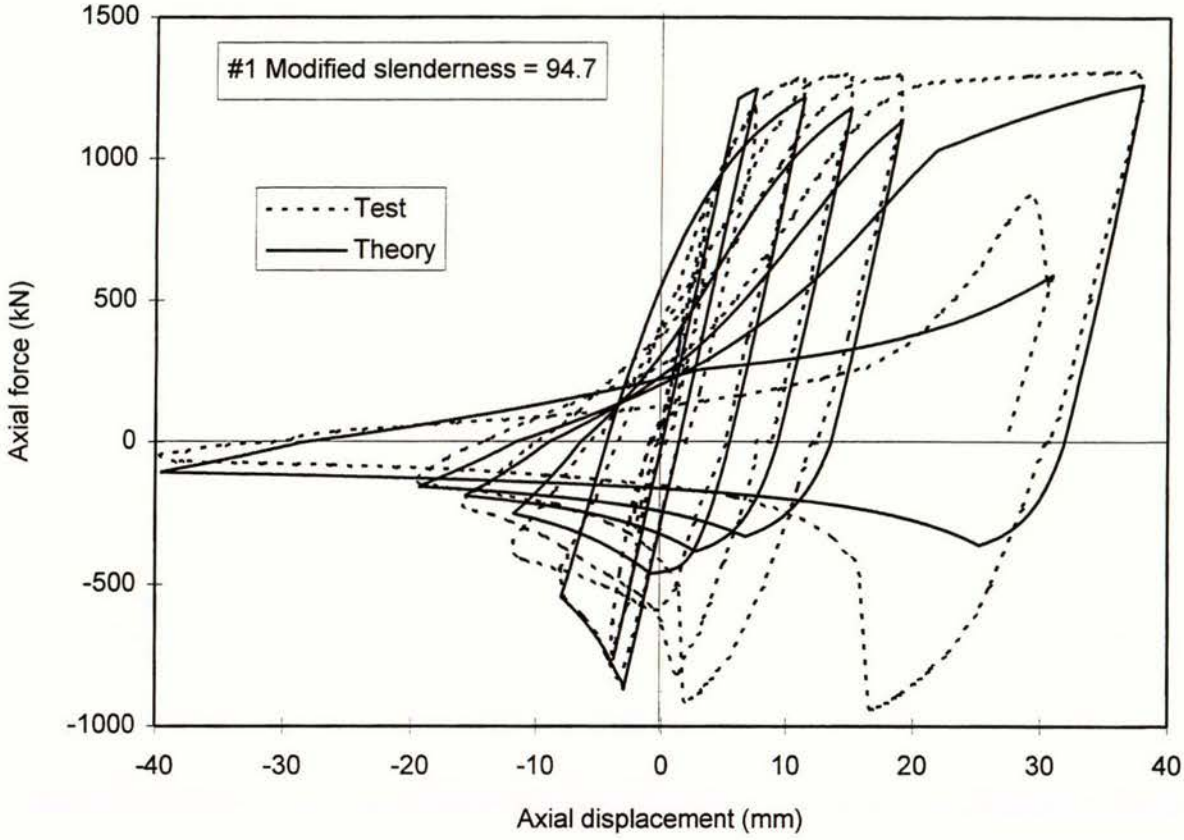

Figure 5.1 Specimen #1: Axial force versus axial displacement

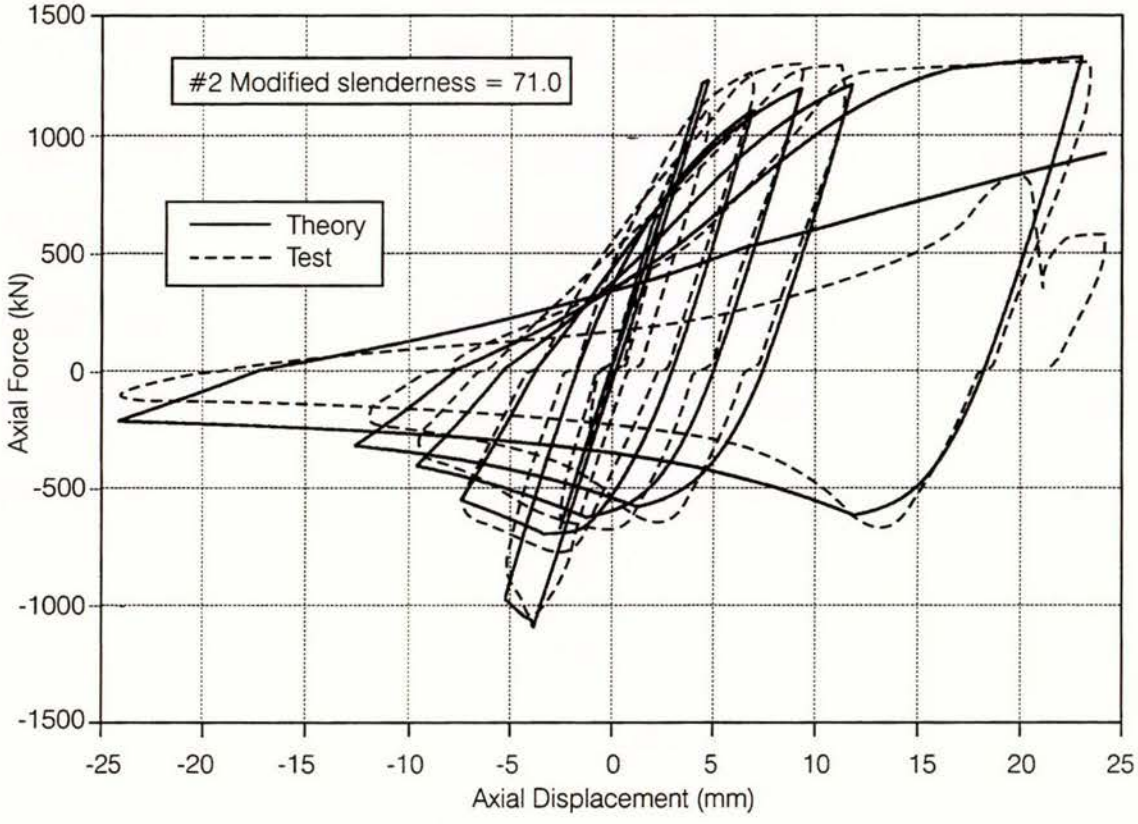

Figure 5.2 Specimen #2: Axial force versus axial displacement

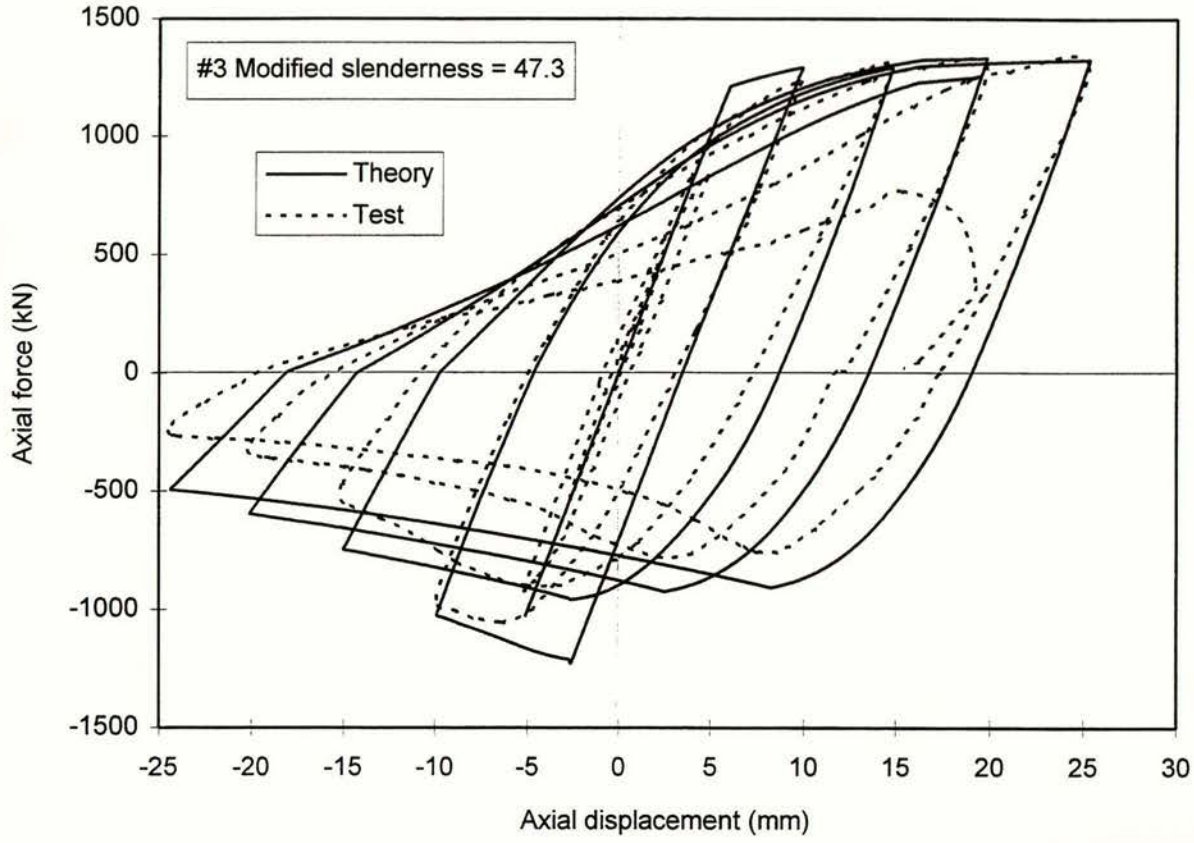

Figure 5.3 Specimen #3: Axial force versus axial displacement

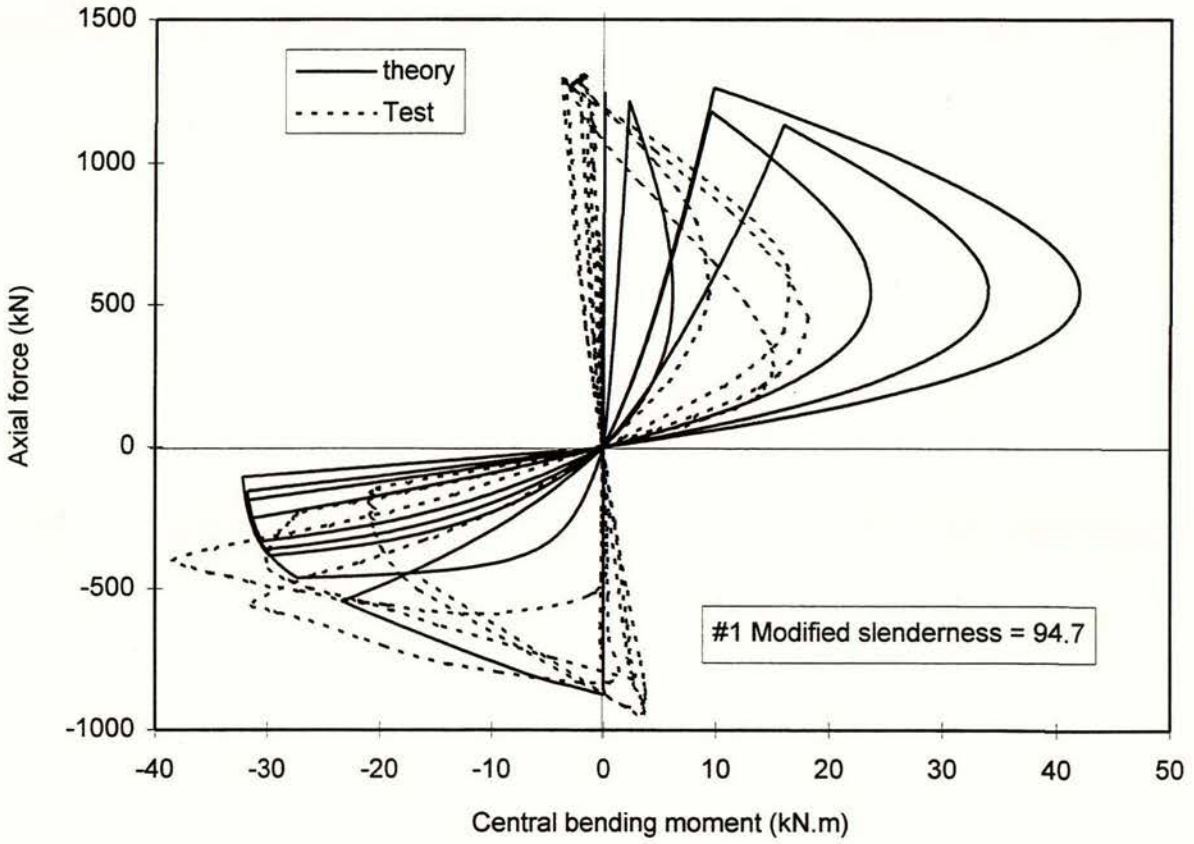

Figure 5.4 Specimen #1: Axial force versus central bending moment

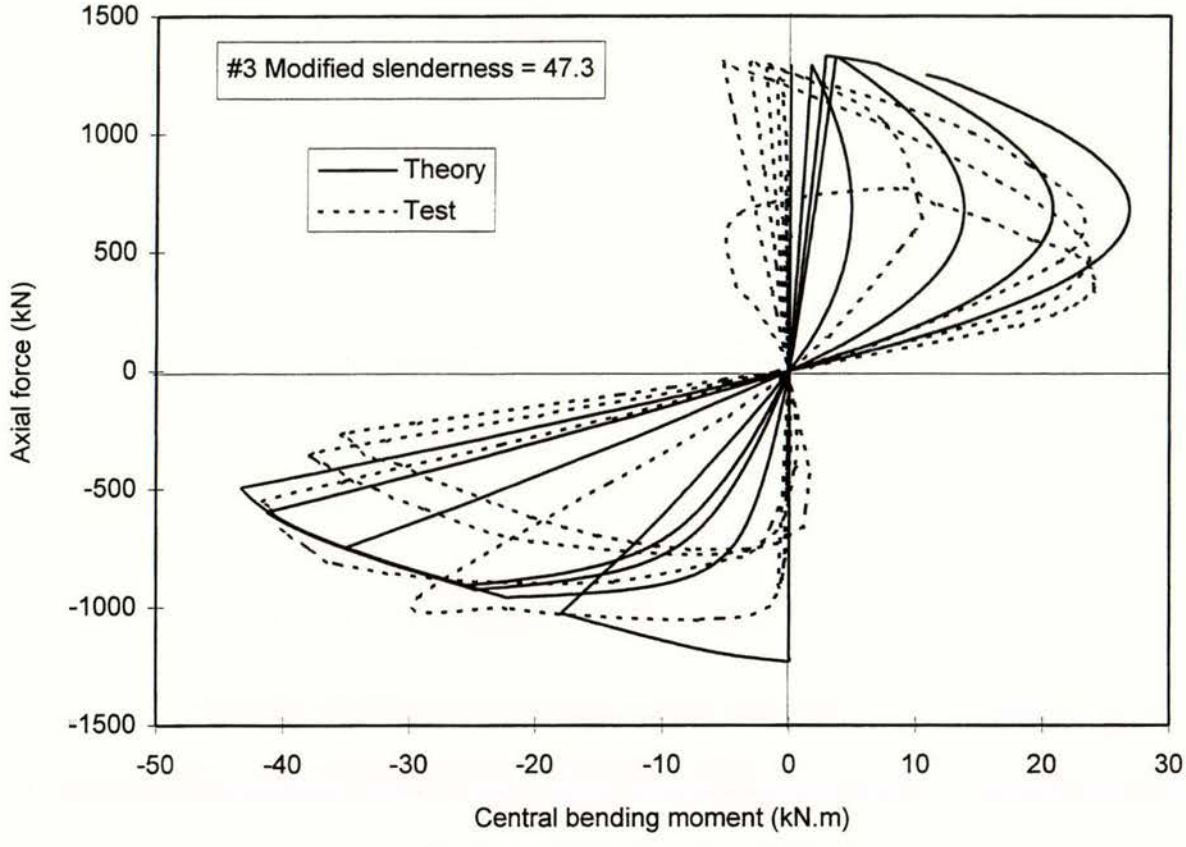

Figure 5.5 Specimen #3: Axial force versus central bending moment

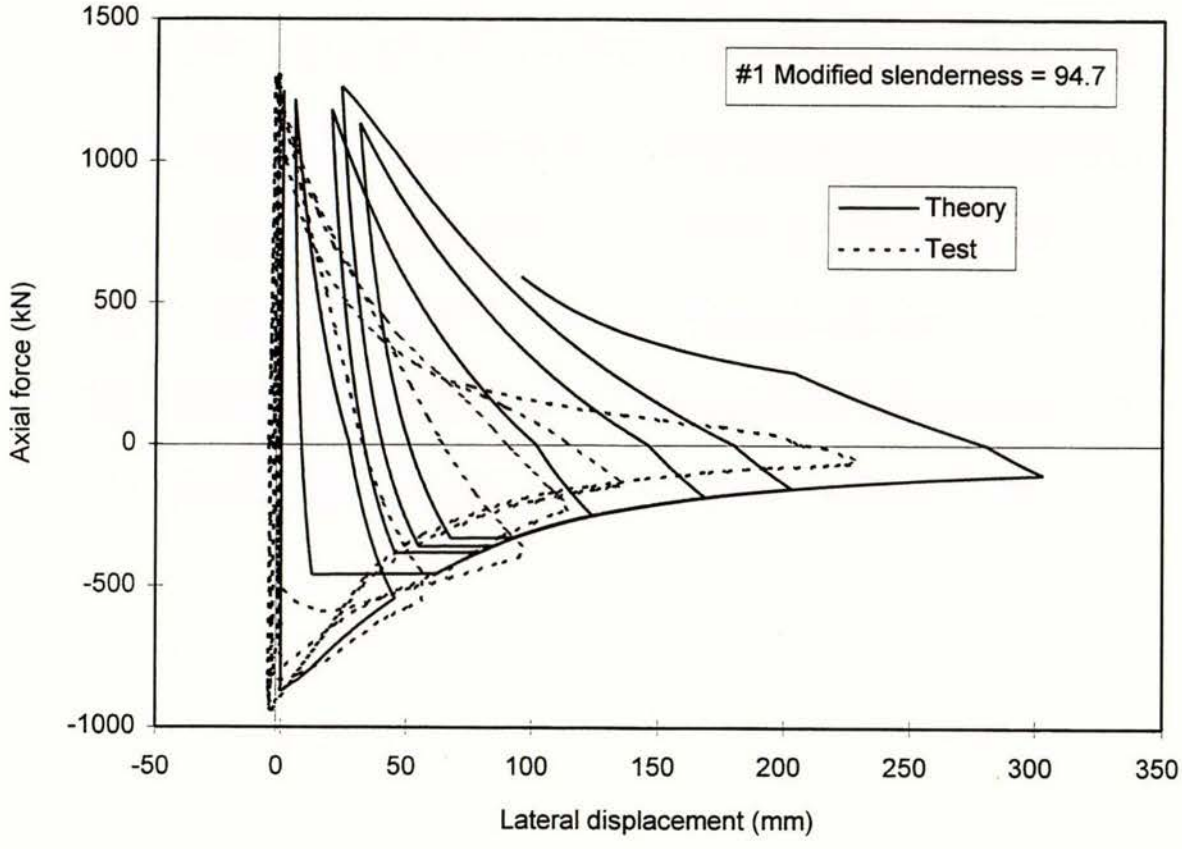

Figure 5.6 Specimen #1: Axial force versus lateral displacement

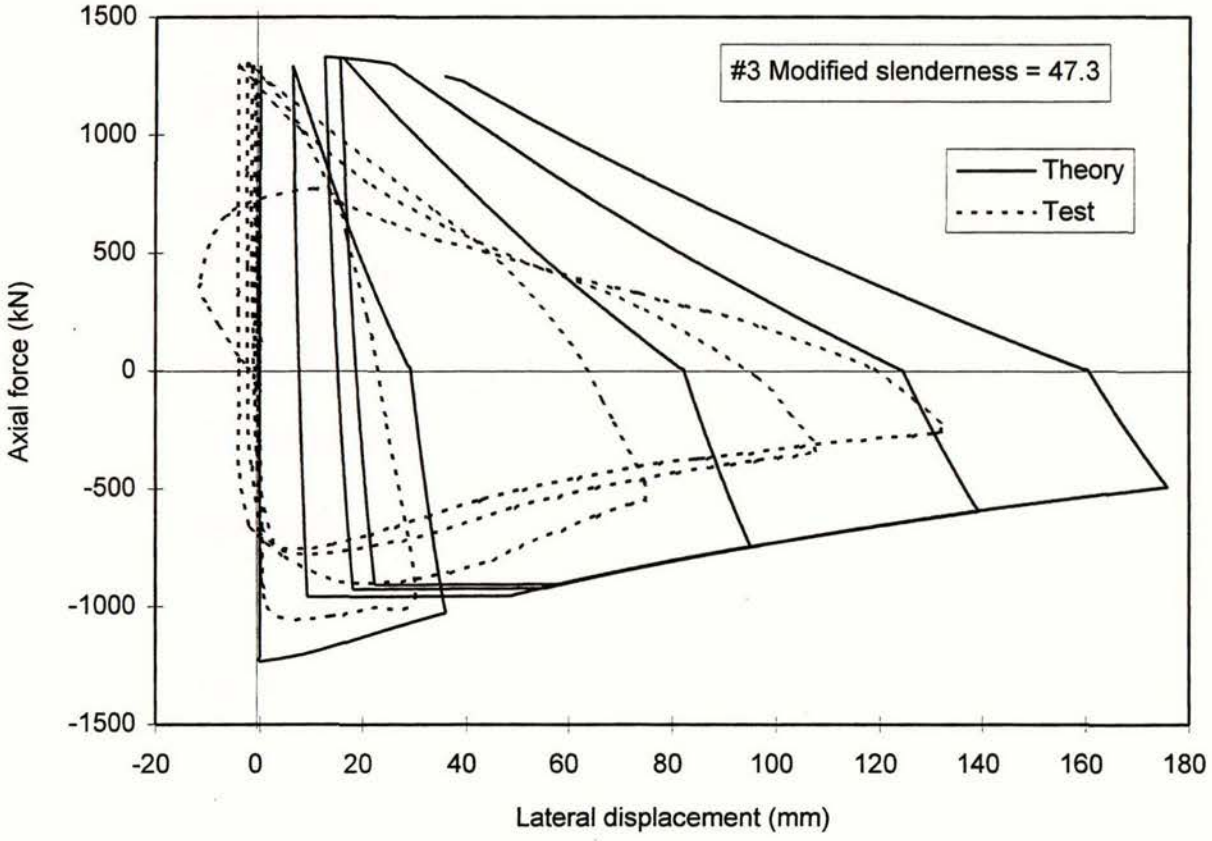

Figure 5.7 Specimen #3: Axial force versus lateral displacement

CHAPTER 6

DISCUSSION

Generally the performance of the members was quite good, but they were significantly less ductile than the Universal Column specimens tested recently [2]. The ductilities of the Rectangular Hollow Section members are compared with the Universal Column members in figure 6.1.

It was found that local buckling occurred relatively quickly and that the magnitude of the local buckles increased under repeated loading. The local buckles had short wave lengths, giving high curvatures and strains, particularly near the corners of the section. Eventually this led to cracks forming near the corners and then spreading into fractures across one side, giving reduced ductilities. This is one of the relatively thicker RHS members and so the performance of many of the thinner RHS members may be even less ductile, because of local buckling occurring relatively earlier.

The agreement between the test and theory curves was very good in general. There were some differences in particular places. It is only possible with the current theoretical modelling, to take average values for the linear approximations to the variation of tangent modulus with stress. In addition, there is no allowance for the reduction of the tangent modulus from cycle to cycle, so it will not be possible to get perfect agreement.

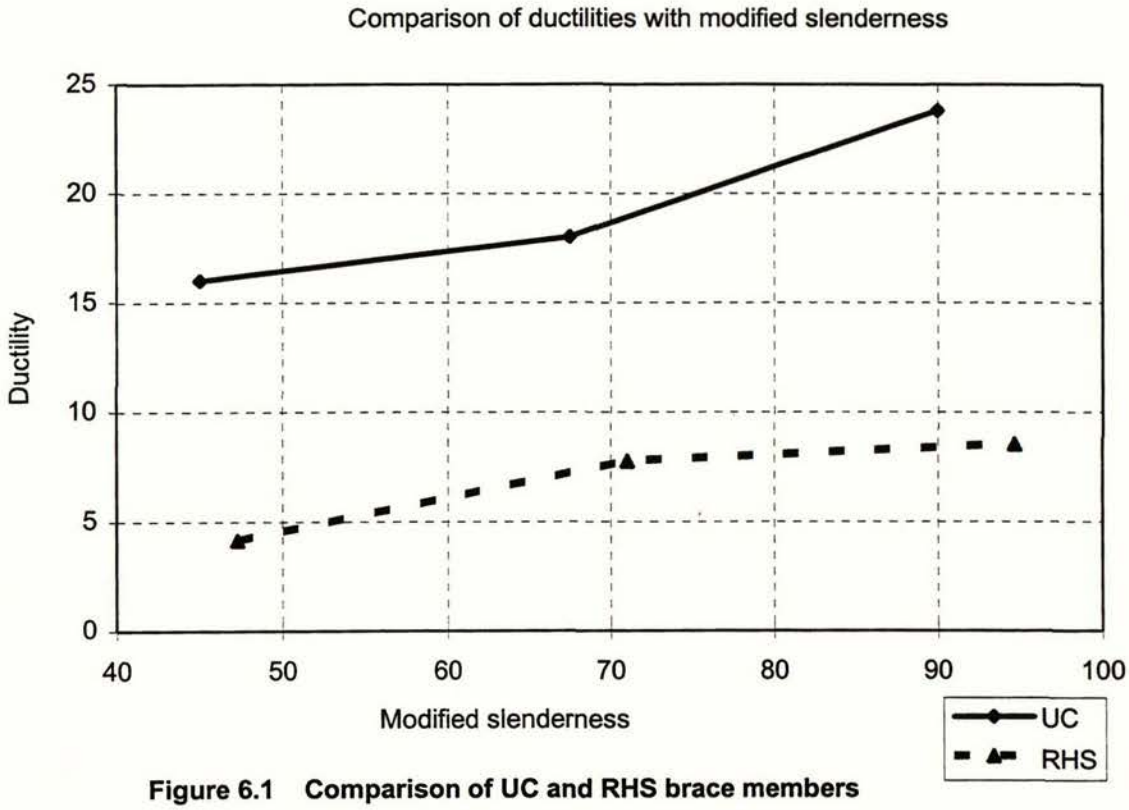

Figure 6.1 Comparison of UC and RHS brace members

CHAPTER 7

CONCLUSIONS

1. The ratio of width to thickness allowed for the elements of cold-formed sections by NZS 3404 Steel Structures Standard may need to be reduced, where high ductility under earthquake-generated forces is required.

2. There was generally good agreement between the theory and test.

3. Stockier members generate fuller hysteresis loops than slender members

4. In slender members the occurrence of local buckling was delayed compared to stockier ones

5. The residual plastic hinge rotation and residual lateral displacement did not disappear even after applying the yield load in tension.

6. The member with the lowest slenderness gave the lowest ductility, because of the relatively earlier occurrence of local buckling.

7. These members made from a rectangular hollow section gave significantly less ductility before failure, compared to some members tested recently made from a universal column section.

REFERENCES

1. NZS 3440:1992; "Steel Structures Standard", Standard Association of New Zealand, Wellington

2. Leowardi, L S and Walpole, W R; "Performance of steel brace members", Research report No 96-3, Civil Engineering Department, University of Canterbury, New Zealand, March 1966

3. American Iron and Steel Institute; "Load and resistance factor design specification for cold-formed steel structural members"; AISI 1991

4. Seismic Provisions for Structural Steel Buildings - Load and Resistance Factor Design American Institute of Steel Construction Inc, Chicago, November 15, 1990

5. Ikeda, K and Mahin, S A; "A refined physical theory model for predicting the seismic behaviour of braced steel frames" Report No UCB/EERC-84/12, Earthquake Engineering Research Center, University of California, Berkeley, California; July 1984

6. Ikeda, K & Mahin, S A; "Cyclic response of steel braces"; Jnl Str Eng, ASCE, v112, n2, p342-361

7. Remennikov, A M and Walpole, W R; "Incremental model for predicting the inelastic behaviour of steel bracing members"; Dept of Civil Engineering, University of Canterbury, Report 95-6, October 1995

8. Popov, E P and Black, R G, "Steel struts under severe cyclic loadings", ASCE, ST9, Sept. 1981

```
·rhs#3.inp
      L       Fyt       Fyc        I         S         A           E     150x100x6 RHS
    2.704   490300.   448800.  4.36D-6  1.02D-4  2.73D-3     200.0D6
    beta    ALFA
    1.3     1.0
     e1     e2    e3    e4
    0.05   0.90 1.2   0.0
    theta0
    0.00`
     k
    0.5
   FLAGSH
    0.0
   SECTION TYPE (1-I sec,2-tube,3-RHS)
    1
   NUMBER OF REVERSALS
   13
   2.4E-03 -2.6E-03 4.9E-03 -5.1E-03 9.9E-03 -9.9E-03 14.8E-03 -15.E-03 19.8E-03
  -20.1E-03 25.3E-03 -24.4E-03 19.3E-03
   1.00E-04 -1.0E-04 1.0E-04 -1.0E-04 1.0E-04 -1.0E-04 1.0E-04 -1.0E-04 1.0E-04
  -1.0E-04 1.0E-04 -1.0E-04 1.0E-04
```

Appendix

Input data for the brace routine.

```
rhs#1.inp
     L       Fyt       Fyc        I         S         A           E     150x100x6 RHS
   2.704   490300.   313800.  4.36D-6  1.02D-4  2.73D-3     200.0D6
   beta    ALFA
   1.3     1.0
    e1     e2    e3    e4
   0.05   0.90 1.2   0.0
   theta0
   0.00
    k
   1.0
  FLAGSH
   0.0
  SECTION TYPE (1-I sec,2-tube,3-RHS)
   1
  NUMBER OF REVERSALS
  15
  1.8E-03 -2.0E-03 3.7E-03 -3.8E-03 7.5E-03 -8.0E-03 11.3E-03 -11.8E-03 15.E-03
 -15.7E-03 19.0E-03 -19.4E-03 37.9E-03 -39.6E-03 31.0E-03
  1.00E-04 -1.0E-04 1.0E-04 -1.0E-04 1.0E-04 -1.0E-04 1.0E-04 -1.0E-04 1.0E-04
 -1.0E-04 1.0E-04 -1.0E-04 1.0E-04 -1.0E-04 1.0E-04
```

```
rhs#2.inp
     L       Fyt       Fyc        I         S         A           E     150x100x6 RHS
   2.028   490300.   393900.  4.36D-6  1.02D-4  2.73D-3     200.0D6
   beta    ALFA
   1.3     1.0
    e1     e2    e3    e4
   0.05   0.90 1.2   0.0
   theta0
   0.00
    k
   1.0
  FLAGSH
   0.0
  SECTION TYPE (1-I sec,2-tube,3-RHS)
   1
  NUMBER OF REVERSALS
  15
  1.2E-03 -1.3E-03 2.3E-03 -2.5E-03 4.8E-03 -5.2E-03 7.0E-03 -7.4E-03 9.4E-03
 -9.64E-03 11.9E-03 -12.6E-03 2.3E-02 -2.42E-02 2.42E-02
  1.00E-04 -1.0E-04 1.0E-04 -1.0E-04 1.0E-04 -1.0E-04 1.0E-04 -1.0E-04 1.0E-04
 -1.0E-04 1.0E-04 -1.0E-04 1.0E-04 -1.0E-04 1.0E-04
```